| | |
|---|---|
| **Titre:** Title: | Analysis of power variation in a CANDU-6 with a loss of moderator |
| **Auteur:** Author: | Yifeng Fan |
| **Date:** | 2007 |
| **Type:** | Mémoire ou thèse / Dissertation or Thesis |
| **Référence:** Citation: | Fan, Y. (2007). Analysis of power variation in a CANDU-6 with a loss of moderator [Mémoire de maîtrise, École Polytechnique de Montréal]. PolyPublie. https://publications.polymtl.ca/8100/ |

UNIVERSITÉ DE MONTRÉAL

# ANALYSIS OF POWER VARIATION IN A CANDU-6 WITH A LOSS OF MODERATOR

YIFENG FAN
DÉPARTEMENT DE GÉNIE PHYSIQUE
ÉCOLE POLYTECHNIQUE DE MONTRÉAL

MÉMOIRE PRÉSENTÉ EN VUE DE L'OBTENTION
DU DIPLÔME DE MAÎTRISE ÈS SCIENCES APPLIQUÉES
(GÉNIE ÉNERGÉTIQUE)
NOVEMBRE 2007

*Your file Votre référence*
*ISBN: 978-0-494-36910-4*
*Our file Notre référence*
*ISBN: 978-0-494-36910-4*

UNIVERSITÉ DE MONTRÉAL

ÉCOLE POLYTECHNIQUE DE MONTRÉAL

Ce mémoire intitulé:

# ANALYSIS OF POWER VARIATION IN A CANDU-6 WITH A LOSS OF MODERATOR

présenté par: FAN YiFeng

en vue de l'obtention du diplôme de: Maîtrise ès sciences appliquées

a été dûment accepté par le jury d'examen constitué de:

M. HÉBERT Alain, D.Ing., président

M. KOCLAS Jean, Ph.D., membre et directeur de recherche

M. MARLEAU Guy, Ph.D., membre

# DEDICATION

To my parents and my wife

# ACKNOWLEDGEMENTS

I cannot thank my supervisor, Professor Jean Koclas, enough for his patience, confidence, support, encouragement, and guidance throughout the preparation of this thesis, and particularly for his insightful advice during times of great difficulty.

I would like to express my appreciation to Professor Alberto Teyssedou and Professor Daniel Rozon for their interesting courses which provided me with my fundamental knowledge in Nuclear Engineering.

I also wish to thank all the members of the Institute of Génie Nucléaire (IGN) group and, in particular, my friends there for establishing a supportive, friendly environment and for always being ready to help each other during the difficult stages of this work.

I am especially grateful to Monchai G. Assawar and Cornelia T. Chilian for their help.

I also wish to thank all the people involved in the DRAGON, DONJON and NDF programs for contributing all their hard work.

Finally, I would like to thank my parents (Chen, JianYuan and Fan, RenGui) and my wife (Qian, Jin), to whom I owe much for their unending patience, encouragement, and understanding. Without their support, I could not have completed this work.

# RÉSUMÉ

Une perte de l'eau lourde du système de modérateur causera les diminutions de niveau du modérateur d'une calandre du réacteur de CANDU-6. Habituellement les interférences des fonctions Baisse Contrôlée de Puissance et Recul Rapide de Puissance au début de la chute du niveau de modérateur assureront l'arrêt du réacteur ou une réduction de puissance du réacteur pendant ce processus transitoire. Si ces deux fonctions étaient indisponibles, le système de régulation du réacteur essayera de compenser la réactivité négative provoquée par la perte de modérateur. Cette compensation pourrait causer un basculement de la puissance, avec une diminution de la puissance dans le haut du réacteur, et une augmentation de la puissance dans le bas du réacteur.

Dans cette analyse, différents taux de fuite de modérateur seront employés pour déterminer les relations entre la puissance et les taux de fuite. Les puissances maximales de grappe, obtenues à partir de l'analyse avec le code DONJON et le code NDF pour un réacteur CANDU-6, se sont avérées insensibles aux taux de fuite de modérateur. La puissance totale dans le coeur de réacteur a une forte corréllation serrée avec la rangée de combustible atteinte par le niveau du modérateur.

De la même manière, l'analyse du taux de fuite de modérateur de 40 l/s montre que, sans les fonctions de STEPBACK et de SETBACK, les basculements sérieux de puissance se produiront pendant la transitoire de quinze minutes. Les puissances maximales de grappes et les puissances maximales de canal atteindront des niveaux plus élevés seulement en raison des actions compensatrices des contrôleurs zonaux. Les mouvements des barres de contrôle empireront ce basculement de puissance.

De cette analyse, on conclura que la puissance maximale de grappe atteinte pendant la perte de modérateur est de 1.18%. Le risque d'assèchement de grappe n'est donc pas très grand.

# ABSTRACT

A loss of heavy water in a postulated small failure in the horizontal unpressurized calandria vessel of a CANDU-6 reactor will lead to a drop in the moderator level in the reactor core. The STEPBACK and SETBACK functions at the initial moment of the drop in moderator level ensure a reactor shutdown and a reduction in total reactor power during this 900 seconds postulated transient. If the STEPBACK and SETBACK functions are unavailable, the reactor's regulating system will try to compensate for the negative reactivity resulting from the loss of the moderator. This kind of compensation will lead to power distortions from top to bottom in the reactor core.

Comparisons of different moderator leakage rates were used in the analysis to determine the relationships between the power and the moderator leakage rates. Maximum bundle and channel powers obtained were insensitive to the moderator leakage rate.

In a complete analysis for a moderator leakage rate of 40 l/s, it was found that, without the STEPBACK and SETBACK functions, serious power distortions would occur during the 900 seconds transient. The maximization of bundle and channel power during this transient happened in the bottom part of the reactor, and the regulating system worsened this power distortion.

From the above analysis, it was concluded that the maximum bundle power attained during the loss of the moderator was 1.18% of its initial value. The risk of bundle dryout was, therefore, quite small.

# CONDENSÉ EN FRANÇAIS

## Objectifs de cette étude

Les réactions neutroniques en chaîne du réacteur CANDU-6 sont soutenues par le ralentissement des neutrons rapides en neutrons thermiques par l'eau lourde (modérateur) dans le cœur du réacteur CANDU-6. Si le coeur du réacteur CANDU-6 perd son modérateur, on observera une diminution de puissance du réacteur pendant cette transitoire de quinze minutes après le début de la perte.

Les barres de contrôle du réacteur CANDU-6 à Gentilly-2 ont été mises sur mode "manuel" quand le réacteur atteint la pleine puissance dans un état stable [1] . La raison de cette opération en mode "manuel" est que les barres de contrôle ne sont pas supposées être extraites du coeur du réacteur quand la puissance du réacteur est élevée.

Nous postulons que les fonctions de STEPBACK et SETBACK seront indisponibles. Pendant la transitoire de quinze minutes, le système de régulation de réacteur, via les barres de contrôles et les contrôleurs zonaux, essayera de compenser la réactivité négative provoquée par la perte supplémentaire de neutrons rapides et thermiques. Cette compensation causera un basculement, avec une diminution de la puissance dans le haut du réacteur, et une augmentation dans le bas du réacteur.

Pendant cette transitoire, l'étude de puissances atteintes sera utilités pour déterminer si les conditions d'opération d'un réacteur de CANDU-6 sont sécuritaires au taux de fuite de modérateur 40 l/s, et quelles conditions d'opération et quelles combinaisons de système

de régulation seront les meilleures. Les combinaisons des systèmes de régulation seront comme suit :

a) Les fonctions de SETBACK sont fonctionnelles, les barres contrôle sont en le mode "automatique".
b) Les fonctions de SETBACK sont fonctionnelles, les barres contrôle sont en le mode "manuel".
c) Les fonctions de SETBACK ne sont pas fonctionnelles, les barres de contrôle sont en mode "automatique".
d) Les fonctions de SETBACK ne sont pas fonctionnelles, les barres de contrôle sont en mode "manuel".

Les puissances de grappe seront étudiées à différents taux de fuite du modérateur, comme par exemple 10 l/s, 20 l/s, 40 l/s, 80 l/s et 122 l/s.

Finalement une analyse complète de la condition opérationnelle sera effectuée pour le taux de fuite de modérateur 40 l/s. À l'intérieur de cette analyse, les mouvements de contrôleurs zonaux, les puissances régionales et les puissances de grappe et de canal seront étudiées.

## Théorie

L'équilibre entre la production et la destruction des neutrons dans chaque de élément volume microscopique mène à un ensemble d'équations de transport neutronique. De ces équations, les équations de diffusion des neutrons pour le coeur du réacteur au complet

seront obtenues par les approximations P1 [2]

Les équations de cinétique et pace tempo comptent deux series d'équations: La première série équation décrit le flux de neutron, et la deuxième série d'équations décrit les concentrations de précurseurs des neutrons retardés.

Finalement il y a deux genres d'équations de diffusion neuronique à résoudre. Le premier type d'équations est donné par les équations statiques de diffusion neutronique; et le deuxième type étant donné par les équations cinétiques. On emploiera différentes méthodes d'itération pour trouver leurs solutions. La méthode implicite sera employée pour les solutions intégrales des équations cinétiques de diffusion neutronique. Les calculs stationnaires servent de conditions initiales dans la simulation de cinétique espace-temps.

Habituellement deux groupes d'énergie des neutrons seront suffisants pour les calculs de diffusion neutronique d'un grand réacteur tels le CANDU-6 [2]. Aussi on utilisera la méthode de différence finie centrée pour les discrétisations spatiales et une méthode implicite pour le temps. Par cette discrétisation des variables spatiale et temporelle, un ensemble d'équations algébriques couplées sera résolu pour obtenir le flux initial.

## Les logiciels

Les programmes de calculs neutroniques statiques sont principalement employés pour déterminer et calculer les flux et Keff statiques initiaux. Ils seront egalement employés pour calculer quelques paramètres dynamiques au moment initial de la simulation

cinétique d'espace-temps. Les calculs cinétiques sont principalement déterminés par le changement des conditions de frontière et des positions des différents mécanismes de réactivité de régulation.

Dans cette recherche, le programme DONJON et le programme NDF seront employés. Le programme DONJON et le programme NDF ont différentes fonctions, mais ils ne peuvent pas être séparés complètement.

Avec le programme CLE-2000 , les modules dans DONJON et dans NDF peuvent être employés à l'analyse des simulations relatives des calculs statiques et cinétiques dans un réacteur CANDU-6 pour la simulation de la perte de modérateur. Aussi les paramètres nucléaires tels que la section efficace macroscopique et le coefficient de diffusion macroscopique seront pré-calculés par le logiciel DRAGON [3]. Le code DRAGON peut employer certaines bibliothèques spécialisées, basées par exemple sur ENDF-B VI [4] pour exécuter les calculs de transport neutronique et pour la condensation en énergie et l'homogénéisation en espace afin de produire les sections efficaces pour les deux groups d'énergie et des coefficients de diffusion, qui seront employés pour résoudre les équations de diffusions neutronique.

## a) Les calculs statiques

Les calculs statiques neutronique sont principalement employés pour l'établissement des sections efficaces macroscopiques des mélanges, des paramètres des neutrons retardés, des paramètres du système de régulation du réacteur, et des paramètres des systèmes de détection de puissances neutroniques.

## b) Les programmes cinétiques

Les calculs cinétiques seront exécutés à partir de la supposition que les conditions frontières changent avec les temps. Les mélanges des mailles, au-dessus du niveau de modérateur seront mis à zéro. Ceci signifiera que les parties au-dessus du niveau de modérateur dans le coeur du réacteur deviendront vides, et aucun flux et aucune puissance ne seront générés dans ces parties au-dessus du niveau du modérateur.

## Les résultats de calculs

Dans cette recherche, beaucoup de calculs de simulation ont été exécutés, ce qui inclut les calculs statiques et les calculs cinétiques. Toutes les différentes méthodes, ce qui incluent les différentes mailles et les différents dispositifs de réactivité etc., sont employés pour exécuter les calculs de référence pour le CANDU-6.

Même si le calcul statique de diffusion neutronique n'est pas l'objet principal de cette thèse, les résultats relatifs seront utiles aux calculs cinétiques subséquents.

## a) Les essais

1) Pendant quinze minutes de transitoire liées à une perte de modérateur dans le coeur du réacteur, quelque fois il pourrait être conclu que la puissance totale de

réacteur aurait des diminutions évidentes, bien que le Keff statique ne diminuerait pas.

2) Avec différents modèles tels que les différentes mailles, les pas de temps et les conditions initiales, les résultats cinétiques démontrent que la stabilité du processus cinétique de calcul neutronique à pleine puissance est atteinte avec le système de régulation, quand il y a aucune perte de modérateur. Si les systémes de régulation n'interfèrent pas, les résultats cinétiques de calcul neutronique pour un réacteur à pleine puissance auront quelques erreurs d'arrondi.

3) En employant la méthode des différences finies centrées, comparées aux mailles 156x156x84, les calculs statiques démontrent que les mailles 104x104x56, sont suffisants pour les calculs cinétiques neutronique. Les déviations moyennes pendant quinze minutes seront de moins de 5%.

4) Avec l'augmentation des mailles du coeur du réacteur, la durée de calcul augmentera évidemment. Un équilibre entre l'exactitude de calcul et le coût de calcul sera fait.

## b) Quelques résultats cinétiques

1) Pour différentes combinaisons des conditions d'opération au taux de fuite du modérateur 40 l/s, la condition d'opération sans les fonctions de STEPBACK et de SETBACK et les barres de contrôle en mode "manuel" sera choisie comme la condition à étudier en mode principal d'opération. Dans ce cas d'opération, les

puissances maximales de grappes atteindront environ 120% des valeurs des initiales et puis diminueront progressivement. La puissance totale du réacteur diminuera pendant 580 secondes environ.

2) Les différents taux de fuite pendant une perte de modérateur affecteront le temps auquel les puissances maximales de grappes seront atteintes. Plus petit sera le taux de fuite de modérateur, plus lentement les puissances maximales de grappes seront atteintes. Les amplitudes des puissances maximales de grappes pendant quinze minutes ne sont pas sensibles aux taux de fuite. Pour le taux de fuite de modérateur de 20 l/s, les puissances maximales de grappes atteindront environ 110 % de la puissance maximale initiale de grappes ; pour le taux de fuite de modérateur de 10 l/s, elles n'ont presque aucun changement pendant 15 minutes ; pour d'autres taux de fuite de modérateur, elles atteindront toujours environ 120% de la puissance maximale initiale de grappes.

3) La puissance totale du réacteur diminue significativement quand les deux premières couches de combustibles sont découvertes. La puissance finale du réacteur à quinze minutes dépendra des taux de fuite. Plus petit sera le taux de fuite de modérateur, plus petite sera la puissance finale du réacteur.

4) Pour le taux de fuite du modérateur de 40 l/s et sans l'interférence des barres de contrôle, les résultats cinétiques démontrent que la puissance maximale de grappe et la puissance maximale de canal apparaîtraient environ en même temps, c'est a dire à 580 secondes. Aussi le maximum de puissance régionale de la zone 5 est atteinte à ce moment. Les temps croissants de puissances maximum de grappe et

de puissances maximales de canal correspondent à celle de la puissance régionale pendant le processus transitoire de quinze minutes.

5) Pour le taux de fuite du modérateur de 40 l/s et sans l'interférence des barres de contrôles, les résultats cinétiques démontrent qu'un basculement de puissance apparaîtrait dans le réacteur. Une diminution de la puissance dans le haut du réacteur et une augmentation de la puissance dans le bas du réacteur apparaissent. Après un certain temps, la puissance maximale sera environ de 80% de la pleine puissance.

# TABLE OF CONTENTS

# LIST OF FIGURES

# LIST OF TABLES

# LIST OF SYMBOLS

| Symbol | Meaning | Unit |
|---|---|---|
| $C_i$ | Precursor concentration of group i | $[cm^{-3}]$ |
| D | Diffusion coefficient | [cm] |
| J | Current density | $[cm^{-2} \cdot ev^{-1} \cdot s^{-1}]$ |
| R | Radius of circle section in CANDU reactor | [mm] |
| t | Actual moderator leakage time | [s] |
| $T_{total}$ | Supposed moderator leakage time | [s] |
| $T_S$ | Time step | [s] |
| $S_{section}$ | Section in a circle | $[cm^2]$ |
| v | Neutron velocity | $[cm \cdot s^{-1}]$ |
| $X_{n+1}$ | Detector responses at this moment | [--] |
| $Y_n$ | Filtered detector responses at previous moment | [--] |
| $Y_{n+1}$ | Filtered detector responses at this moment | [--] |

| | | |
|---|---|---|
| $\beta_i$ | Effective delayed-neutron fraction | $[--]$ |
| $\lambda$ | Eigenvalue | $[--]$ |
| $\nu$ | Average number of neutrons produced per fission | $[--]$ |
| $\Sigma_f$ | Macroscopic fission cross section | $[cm^{-1}]$ |
| $\Sigma_S$ | Macroscopic scattering cross section | $[cm^{-1}]$ |
| $\Sigma_t$ | Macroscopic total cross section | $[cm^{-1}]$ |
| $\Phi(r,E,\vec{\Omega},t)$ | Angular flux density | $[cm^{-2}\cdot ev^{-1}\cdot sr^{-1}\cdot s^{-1}]$ |
| $\phi(\vec{r},E,t)$ | Scalar flux density | $[cm^{-2}\cdot ev^{-1}\cdot s^{-1}]$ |
| $\phi(\vec{r},t)$ | Macroscopic scalar flux | $[cm^{-2}\cdot s^{-1}]$ |
| $\psi(\vec{r},E)$ | Microscopic distribution | $[cm^{-2}\cdot ev^{-1}]$ |
| $\tau$ | Delay time | $[s]$ |
| $\chi_i^d$ | Delayed neutron spectrum | $[--]$ |
| $\chi^P$ | Prompt fission neutron spectrum | $[--]$ |
| $\overrightarrow{\Omega}\cdot$ | Solid angle (direction of motion) | $[sr]$ |

Matrix of the neutron velocity..... $[cm \cdot s^{-1}]$

$$[v] = \begin{bmatrix} v_1 & & & \\ & v_2 & & \\ & & . & \\ & & & v_G \end{bmatrix}$$

Square matrix of cross section..... $[cm^{-1}]$

$$[\Sigma] = \begin{bmatrix} \Sigma_{t1} - \Sigma_{S1\leftarrow 1} & -\Sigma_{S1\leftarrow 2} & \cdots & -\Sigma_{S1\leftarrow G} \\ -\Sigma_{S2\leftarrow 1} & \Sigma_{t2} - \Sigma_{S2\leftarrow 2} & \cdots & -\Sigma_{S2\leftarrow G} \\ . & . & . & . \\ -\Sigma_{SG\leftarrow 1} & -\Sigma_{SG\leftarrow 2} & \cdots & \Sigma_{tG} - \Sigma_{SG\leftarrow G} \end{bmatrix}$$

Vector of the prompt energy spectrum..... $[--]$

$$[\chi^p] = \begin{bmatrix} \chi_1^p \\ \chi_2^p \\ . \\ \chi_G^P \end{bmatrix}$$

Vector of $\nu$ times the fission cross section..... $[cm^{-1}]$

$$[\nu\Sigma_f] = \begin{bmatrix} \nu\Sigma_{f1} \\ \nu\Sigma_{f2} \\ . \\ \nu\Sigma_{fG} \end{bmatrix}$$

Vector of delayed neutron spectra..... $[--]$

$$[\chi_i^d] = \begin{bmatrix} \chi_{i1}^d \\ \chi_{i2}^d \\ . \\ \chi_{iG}^d \end{bmatrix}$$

Matrix of diffusion coefficient..... $[cm]$

$$[D]=\begin{bmatrix} D_1 & & & \\ & D_2 & & \\ & & . & \\ & & & D_G \end{bmatrix}$$

Vector of fluxes..... $[cm^{-2} \cdot s^{-1}]$

$$[\phi]=\begin{bmatrix} \phi_1 \\ \phi_2 \\ . \\ \phi_G \end{bmatrix}$$

Coefficient matrix..... $[--]$

$$[H]=\begin{bmatrix} [H]_{11} & [H]_{12} \\ [H]_{21} & [H]_{22} \end{bmatrix}$$

Vector of flux and precursor..... $[cm^{-2} \cdot s^{-1}]$

$$[\Psi]=\begin{bmatrix} [\Phi_1] \\ [\Phi_2] \\ [.] \\ [\Phi_G] \\ [C_1] \\ [C_2] \\ [.] \\ [C_D] \end{bmatrix}$$

# LIST OF ABBREVIATIONS

CANDU.....Canada deuterium uranium

CCSI.....Cyclic Chebyshev Semi-Iterative

CPLOG.....Set-point of logarithmic power

ERPU.....Power error

ERPU1.....The power term component of the power error

ERPU2.....The rate term component of the power error

FPP.....Full percent power

PLGCA.....Calibrated logarithmic power

RRS.....Reactor regulating system

# CHAPTER 1: INTRODUCTION

## 1.1 Objective of this research

The chain reaction of a CANDU-6 reactor relies on the slowing down of fast neutrons by heavy water in an unpressurized calandria containing the moderator. The presence of a radial reactor reflector is necessary to keep the reactor critical. The objective of this study was to assess, with the use of a hypothetical breach of the calandria, the severity of bundle and channel dryout risk in the reactor when a loss of the moderator occurs.

A loss of heavy water in a CANDU-6 reactor core precipitates a predictable sequence of events: the level of moderation drops, the fast neutrons no longer decelerate enough to maintain the reactor's criticality, the fission reactions decrease correspondingly and, as a consequence, the total reactor power decreases.

With the compensations from various reactivity control devices, some regional powers will increase. When the regional powers increase to 108% or more of FPP, the STEPBACK function intervenes (in our simulations, sometimes this function is inhibited to avoid the expense of a reactor shutdown) and then the SETBACK function, leading to an immediate total reactor power decrease. If the regional powers continue increasing above 122.2% of FPP, the two shutdown systems SDS1 and SDS2 intervene [5].

The STEPBACK function rapidly reduces the total reactor power to zero with the help of four mechanical absorber rods from SDS1. The SETBACK function reduces the total reactor power to 60% in the presence of a power tilt. If the STEPBACK and SETBACK functions are available during a loss of moderator, the risk of the bundles and channels

drying out will be very low [1].

In our selection of a safe operation mode, we took into account the SETBACK function, adjuster operation mode and liquid zone controllers. The adjusters and liquid zone controllers were moved to compensate for the negative reactivity resulting from the loss of moderator. A top to bottom flux distortion in the reactor core was generated: the power decreased in the top half of the reactor core and increased in the bottom half.

The movement of the reactivity control devices, especially the liquid zone controllers, in the CANDU-6 reactor is controlled by the reactor regulating system (RRS). Making alterations to the standard control rules (for example, the restriction of the movement of adjusters) allowed us to reflect plant operating practices and gave us more conservative and safer simulation results.

The maximum bundle powers and the maximum channel powers are of greatest interest within a prescribed power limit and should be assessed if the kind of failure we postulated leads to ruptures due to the drying out of the fuel bundles and channels. If this should happen, a number of fission products would be released into the reactor coolant circuit. And, if the calandria tube integrity were to be threatened by the increase of the bundle powers, a large number of fission products would be released into the moderator system. All of these hypothetical failures and events make it essential to calculate these maximum bundle powers and maximum channel powers during the 900 second transient resulting from a loss of moderator.

## 1.2 Review of CANDU-6 Reactor

In the fuel assemblies of a CANDU-6 reactor, coolant flows over the surface of the fuel pins inside pressure tubes. $CO_2$ fills the space between these pressure tubes and their surrounding calandria tubes.

Each cell in this reactor contains one fuel assembly, referred to as the cell lattice. A standard CANDU-6 cell dimension is 28.57 cm along the y and x axes, and about 50 cm along the z axis. Each of the reactor's 380 fuel channels contains 12 fuel bundles, giving this reactor a total of 4560 fuel bundles. The CANDU-6 has two shutdown systems and a set of regulating system rules. A cut-out view of the CANDU-6 reactor is shown in Figure 1.1.

Our simulations were based on this prototype of the CANDU-6 reactor. The reactivity control devices we used in our simulation are those presented in Figure 1.1.

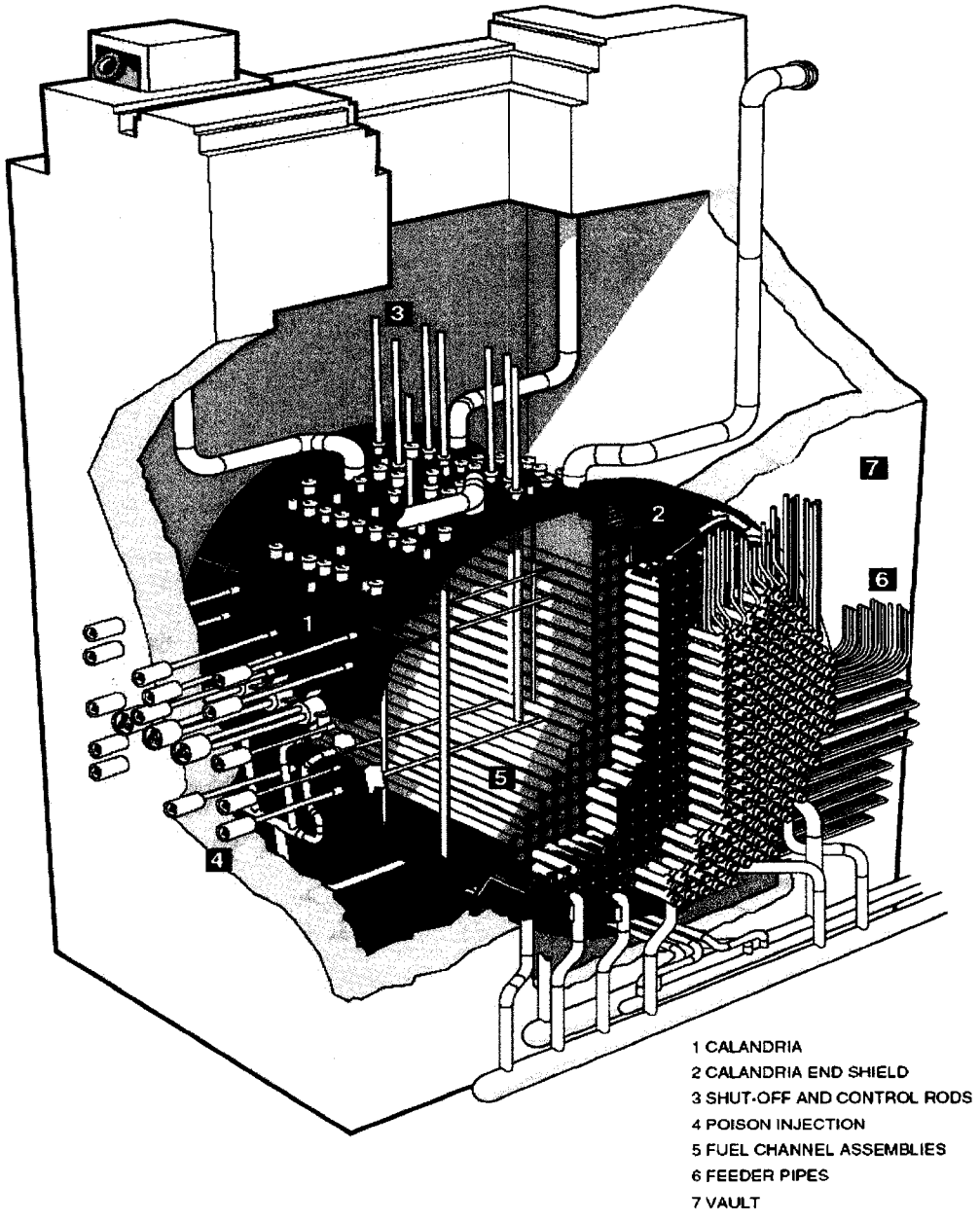


**Figure 1.1 CANDU-6 reactor assembly** (from http://canteach.candu.org)

## 1.3 Review of the moderator system

Heavy water in a CANDU-6 reactor calandria is the moderator used to slow down the fast neutrons in order to release thermal energy. The use of this particular moderator in a CANDU-6 reactor permits the use of natural uranium.

The calandria tubes isolate thermally the heavy water moderator at about 70 degrees Celsius from the pressure tubes, which are at about 310 Celsius degrees. The moderator in a CANDU-6 reactor is usually under one atmosphere pressure plus its own hydrostatic pressure.

The moderator is maintained at a constant temperature and at a high isotopic concentration, both of which will affect the criticality of a CANDU-6 reactor. In normal operating mode, the heat generated in the moderator in a CANDU-6 reactor calandria is produced by the neutron capture, neutron deceleration, and gamma ray interactions. The heat will finally be taken out by the moderator heat exchangers, as shown in Figure 1.2.

The chemistry of the moderator in a CANDU-6 reactor is controlled to minimize the radioactivity produced by deuterium and corrosion products. A moderator purification system is provided to maintain moderator water purity. Usually, the heavy water's isotopic concentration is kept at 99.75% or higher.

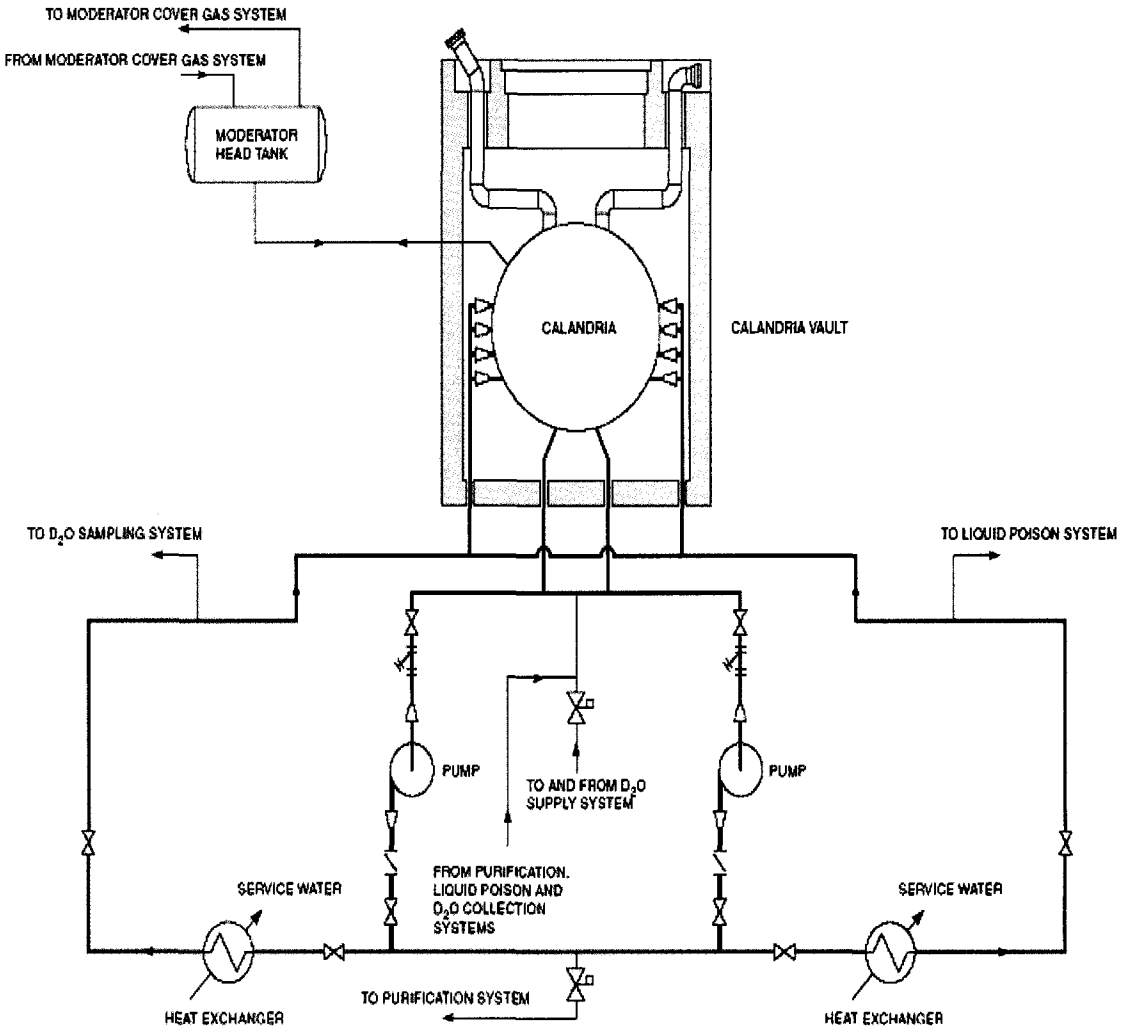


**Figure 1.2 CANDU-6 moderator system** (from http://canteach.candu.org)

In our simulations, we disregarded the two relief pipes above the reactor calandria; that is, we considered the moderator only inside the reactor calandria. These details are shown in Figure 1.2.

## 1.4 Review of DONJON and NDF

Since it is impossible to solve the transport equation for the complete geometry of a CANDU-6 reactor core, the method of the separation of flux will be considered,

$$\phi(\vec{r},E,t)=\phi(\vec{r},t)\cdot\psi(\vec{r},E) \qquad \text{EQ 1.1}$$

where

$\phi(\vec{r},E,t)$: Scalar flux density;

$\phi(\vec{r},t)$: Macroscopic scalar flux;

$\psi(\vec{r},E)$: Microscopic flux distribution from the cell calculation [2]

The microscopic cross section was used in the related lattice cell calculations, in which the transport equation is solved by collision probabilities. The flux distributions of the related cells were obtained from the DRAGON code. [6] This lattice cell calculation provides macroscopic cross sections and diffusion coefficients for diffusion calculation in the reactor. The spatial homogenization eliminates the geometric description of the cells during the related neutron diffusion calculations. For the static neutron diffusion calculations [2], two energy groups were considered sufficient for the large size thermal reactor such as CANDU-6. Six groups of delayed neutrons were used for the related space-time kinetics neutron diffusion calculations.

Modules of the DONJON and NDF codes were used for the numerical solution of the neutron diffusion for the whole reactor. In the simulations, DONJON facilitated the

manipulation of the macroscopic cross section data from the DRAGON code. Modules of the NDF code were used to calculate the flux distribution in time and space. Fully implicit time integration and mesh centred finite difference were used.

## 1.5 Review of control devices and detectors

The simulation of reactivity control devices and flux detectors required both DONJON and NDF. Along with the initial flux distributions for the whole CANDU-6 reactor, calculated with the NDF code, initial reference flux readings for the related flux detectors were obtained. The other basic functions of the reactivity control devices and flux detectors were performed in the NDF code with RRS modules. In Figure 1.3, the conceptual layouts of liquid zone control devices and flux detectors are illustrated.

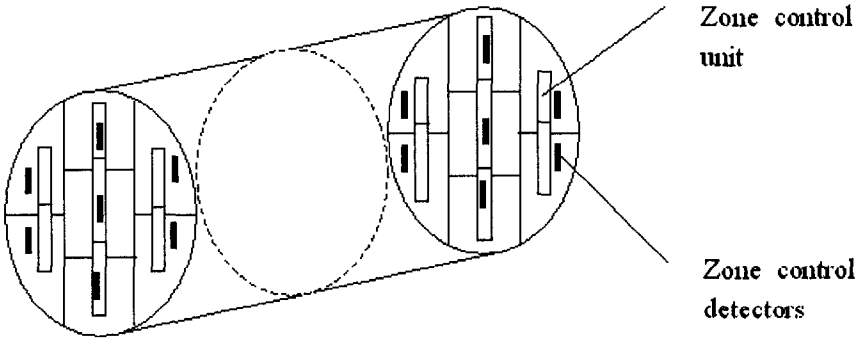


**Figure 1.3 Layout of liquid controllers and flux detectors**

Three kinds of detectors regulate a reactor's power: 2 ion chambers, 28 platinum detectors and 102 vanadium detectors. The reactor regulating systems include 14 liquid zone controllers, 21 adjusters and 4 mechanical control absorbers. [5]

A typical layout of zonal powers is shown in Figure 1.4, where we can see that a symmetrical zonal layout exists between zones 1 to 7 and zones 8 to 14 along the z axis. Also, zones 1 and 2 are symmetric with zones 6 and 7 respectively.

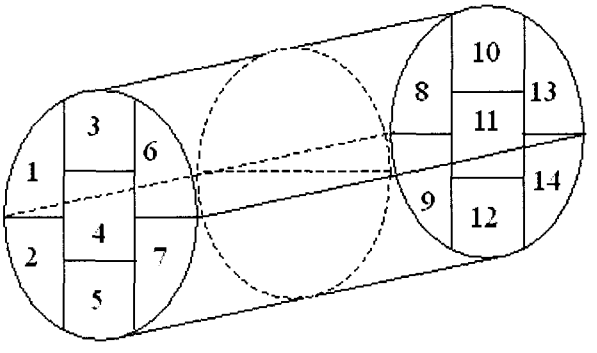


**Figure 1.4 Layout of zones**

## 1.6 Contributions of this thesis

A postulated small event in the horizontal unpressurized calandria vessel of a CANDU-6 reactor resulted in a moving surface of heavy water at the top of the horizontal cylinder.

This was modeled as a moving boundary condition applied to the three dimensional space-time kinetic equations in the diffusion theory. The transients lasted 900 seconds.

Operating expenses in some CANDU-6 plants dictate that the adjusters be left in "manual" mode. The basic idea of this operation selection is that the adjusters are not expected to move when the reactor power is at a higher power and undesirable power peaks are avoided.

In our simulations, the two shutdown systems and the automatic extraction of adjusters in a CANDU-6 reactor were deactivated. If the two shutdown systems intervened, the restart-up of CANDU-6 would be expensive; and if the adjusters intervened, the maximum bundle power during the transient would reach and possibly exceed 120% of its initial value.

The time-dependent diffusion equations were used in these simulations, with two energy groups and six delayed groups of neutron precursors. A simple time-average set of cross sections obtained from the DRAGON code [3] was used to represent the fuel conditions in the core. The properties of the CANDU-6 reactivity devices were also calculated with DRAGON [6].

The mesh centered finite difference was used as the spatial discretisation method, as this is sufficient for CANDU-6 analysis. Time integration was performed with the DONJON/NDF code [7] [8] [9], using a direct fully implicit method [10].

These related results were used to assess the risk of bundle and channel dry out during a loss of moderator.

## 1.7 Organization of this thesis

This thesis is composed of six chapters. The current chapter presents the topic of this project and a review of the CANDU-6 reactor core, related systems and codes used in the modelization.

In chapter 2, a mathematical description of the moderator level dropping is derived; also, we have made a validation of our moderator dropping codes in this postulated failure.

In chapter 3, the related simulation algorithm is discussed; and the static and kinetic parts of our codes are detailed. The moderator level is modeled as a moving boundary condition applied to the three-dimensional space-time kinetics equations in the related diffusion calculation. Various limits of this assumed moving boundary are discussed.

In chapter 4, some static calculation results, such as Keff and the reactivity of various control devices, are reported.

In chapter 5, the results of various operating modes involving various leakage rates are analyzed. The results of one operating mode at the moderator leakage rate of 40 l/s is detailed. The accuracy, speed and stability of the related numerical calculation are also evaluated.

In chapter 6, conclusions and recommendations derived from our analysis are given.

# CHAPTER 2: MODERATOR LEVEL

## 2.1 Model of moderator level

To simplify the simulation of the moderator dropping level, two functions relating the moderator level and the moderator leakage time are presented here. The first one is a linear function relating the moderator level and the moderator-leakage time; the other is a nonlinear function. These two functions affected the simulation results, especially the intervention moment of the regulating systems.

In the simulation, it was assumed that the moderator leakage rates from the CANDU-6 reactor calandria were constant and did not change with time. The function relating the moderator levels in the reactor to the leakage time is really nonlinear, though(!!), because of the circular shape of the CANDU-6 reactor calandria.

Here, the nonlinear function relating the moderator level with time is deduced. The circular section of a CANDU-6 core is shown in Figure 2.1. The differential area dS will be as follows:

$$dS = 2xdy \qquad \text{EQ 2.1}$$

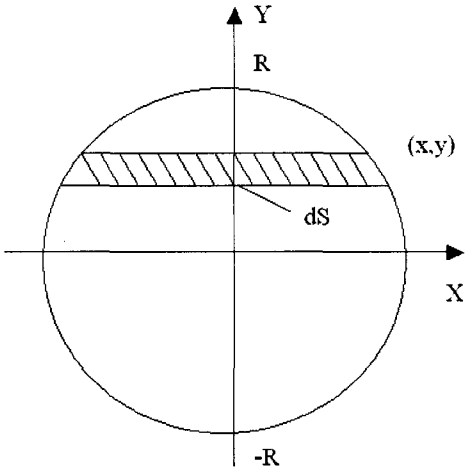


**Figure 2.1 Differential section of reactor core**

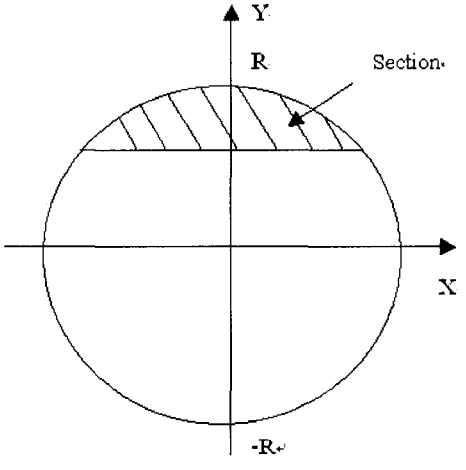


**Figure 2.2 Dropping section during loss of moderator**

From the circular shape of a CANDU-6 reactor, we have:

$$x^2 + y^2 = R^2 \qquad \text{EQ 2.2}$$

Then:

$$S = \int_y^R 2 \times \sqrt{R^2 - y^2}\, dy \qquad \text{EQ 2.3}$$

After the integration of EQ 2.3, a relationship between the dropping section ($S_{section}$) and height (y) can be obtained:

$$S_{section} = 2 \times \left( \frac{y}{2} \sqrt{-y^2 + R^2} + \frac{R^2}{2} \sin^{-1}\left( \frac{y}{R} \right) \right) + C \qquad \text{EQ 2.4}$$

Assuming that the leakage rate is constant, we can deduce the relationship between the moderator level in a CANDU-6 reactor core and the time of moderator leakage:

$$S_{total} \times \frac{t}{T_{total}} = 2 \times \left( \frac{y}{2} \sqrt{-y^2 + R^2} + \frac{R^2}{2} \sin^{-1}\left( \frac{y}{R} \right) \right) + C \qquad \text{EQ 2.5}$$

When t equals to 0, the initial section area is zero.

$$0 = 2 \times \left( 0 + \frac{R^2}{2} \times \frac{\pi}{2} \right) + C$$

Then, we get:

$$C = -\frac{\pi R^2}{2};$$

Where

$S_{total}$ : Total circular area of CANDU-6;

t : The actual moderator leakage time;

$T_{total}$ : The assumed total moderator leakage time;

y : The height of lost moderator.

## 2.2 Validation of moderator level dropping model

Moderator level data for the different leakage rates during this transient are presented in Tables 2.1-2.5. As shown in Figure 2.3, the moderator level perhaps starts to drop from a certain location in the relief pipes and takes a few seconds to descend from that location to the top of the calandria. "Actual time" in the tables refers to the time elapsing as the moderator level drops from the top of the calandria to its current level. These measured data refer to [1].

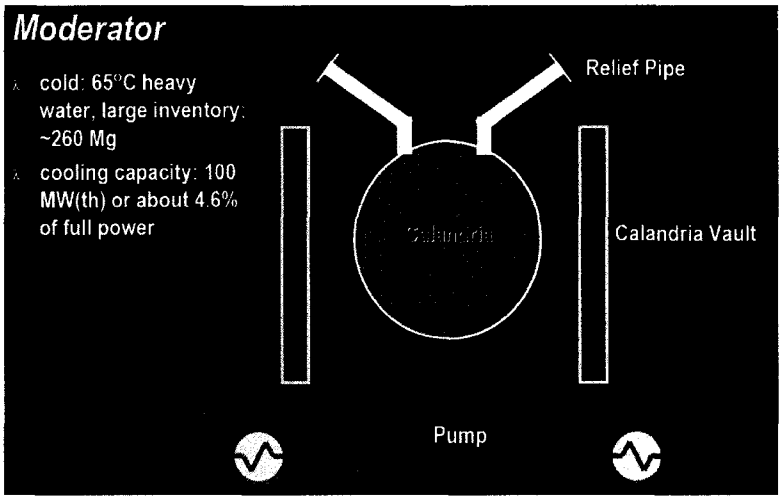


**Figure 2.3 Calandria cut-out section during loss of moderator**

| Moderator level (mm) | Actual time (- 10 seconds) |
|---|---|
| 7595 | 0 |
| 7500 | 5 |
| 7400 | 10 |
| 7300 | 20 |
| 7100 | 40 |
| 6900 | 70 |
| 6800 | 95 |
| 6600 | 130 |
| 6400 | 170 |
| 6200 | 215 |
| 6100 | 240 |

**Table 2.1 Moderator level reductions at leakage rate of 122 l/s [1]**

| Moderator level (mm) | Actual time (- 15 seconds) |
|---|---|
| 7595 | 0 |
| 7260 | 35 |
| 7110 | 55 |
| 7000 | 85 |
| 6900 | 105 |
| 6790 | 135 |
| 6630 | 185 |
| 6470 | 235 |
| 6330 | 285 |
| 6180 | 335 |
| 6000 | 435 |

**Table 2.2 Moderator level reductions at leakage rate of 80 l/s [1]**

| Moderator level (mm) | Actual time (- 30 seconds) |
|---|---|
| 7595 | 0 |
| 7500 | 10 |
| 7400 | 30 |
| 7300 | 55 |
| 7100 | 120 |
| 6900 | 220 |
| 6800 | 280 |
| 6600 | 400 |
| 6400 | 520 |
| 6300 | 610 |
| 6200 | 670 |

**Table 2.3 Moderator level reductions at leakage rate of 40 l/s [1]**

| Moderator level (mm) | Actual time (- 60 seconds) |
|---|---|
| 7595 | 0 |
| 7500 | 15 |
| 7400 | 50 |
| 7300 | 100 |
| 7200 | 162 |
| 7100 | 235 |
| 7000 | 325 |
| 6900 | 450 |
| 6800 | 545 |
| 6700 | 680 |

**Table 2.4 Moderator level reductions at leakage rate of 20 l/s [1]**

| Moderator level (mm) | Actual time (- 100 seconds) |
|---|---|
| 7595 | 0 |
| 7500 | 50 |
| 7450 | 80 |
| 7400 | 138 |
| 7300 | 235 |
| 7250 | 290 |
| 7200 | 352 |
| 7150 | 440 |
| 7100 | 520 |
| 7000 | 680 |

**Table 2.5 Moderator level reductions at leakage rate of 10 l/s [1]**

Using the various models of moderator drop levels in a CANDU-6 reactor core, we

obtain the graphs of the decreasing moderator level. The calculated drop level during this transient is close to the site data from [1], showing that our models of the moderator level were close to actual situations. As the realistic data from [1] didn't last 900 seconds, so the data in Table 2.1 to 2.5 also didn't last 900 seconds. Figure 2.4 is used to confirm the level during a loss of moderator in a CANDU-6 reactor core at the leakage rates of 80 l/s and 122 l/s; and Figure 2.5 is used for the moderator leakage rates of 20 l/s and 10 l/s.

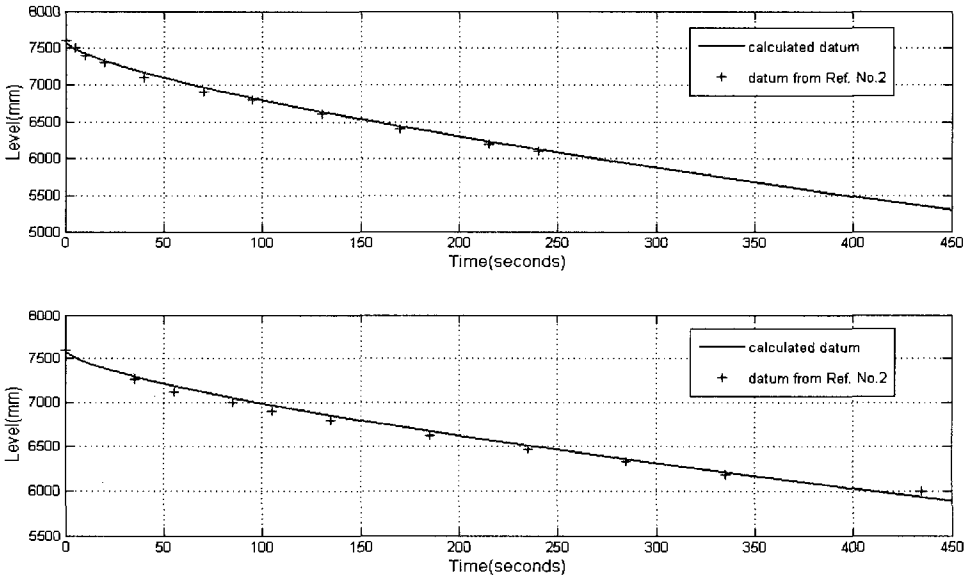


**Figure 2.4 Comparison of moderator levels at leakage rates of 80 l/s and 122 l/s**

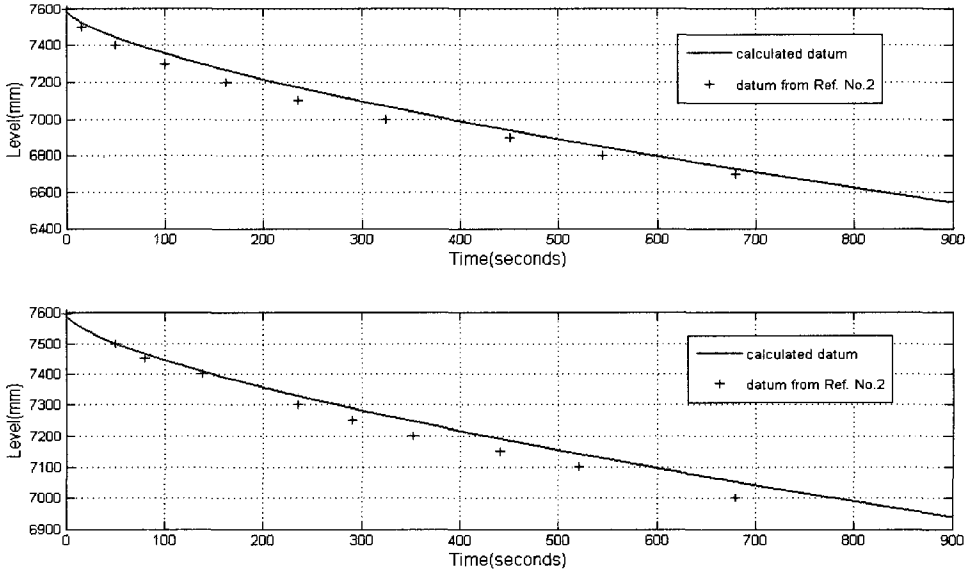


**Figure 2.5 Comparison of moderator levels at leakage rates of 20 l/s and 10 l/s**

The moderator levels affected by different moderator leakage rates are given in Figure 2.6. During this 900 second transient, different moderator levels led to different reactor transients in a CANDU-6 reactor. For example, the different intervention time of the reactivity control devices and shutdown systems led to a final total reactor power loss.

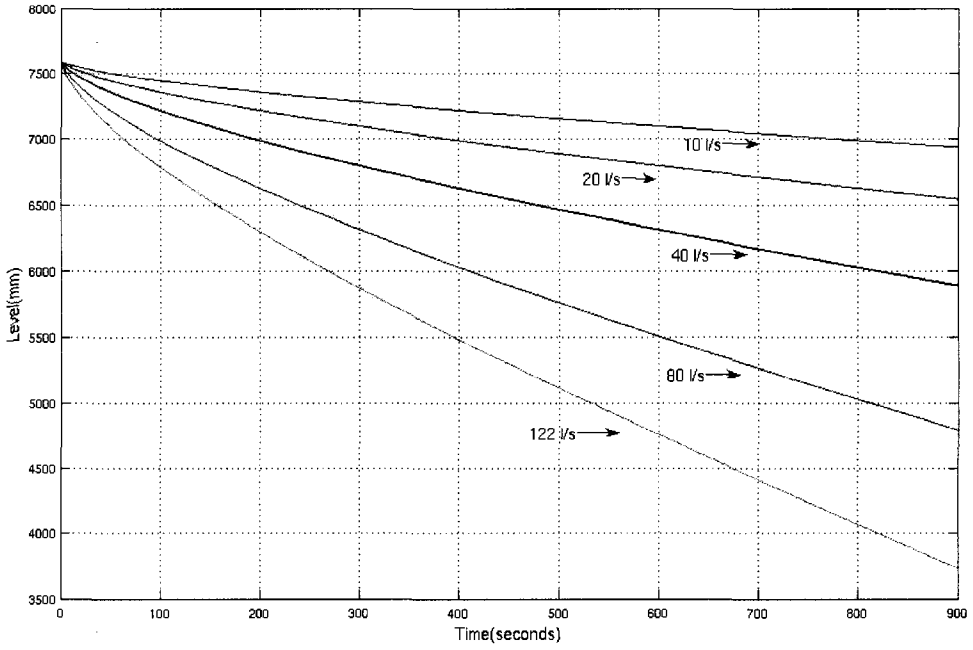


**Figure 2.6 Comparison of moderator levels for various leakage rates**

The moderator leakage rate of 40 l/s was used in most of our research. Also, moderator levels are significantly different in a linear function than in a nonlinear function relating these moderator levels to the leakage time during the 900 second transient. In this thesis, however, the linear function may be ignored because of the circular shape of the calandria in the CANDU-6 reactor. Figure 2.7 shows the differences in linear and nonlinear calculations. If a linear function is supposed to be used, a bigger simulation error will be introduced.

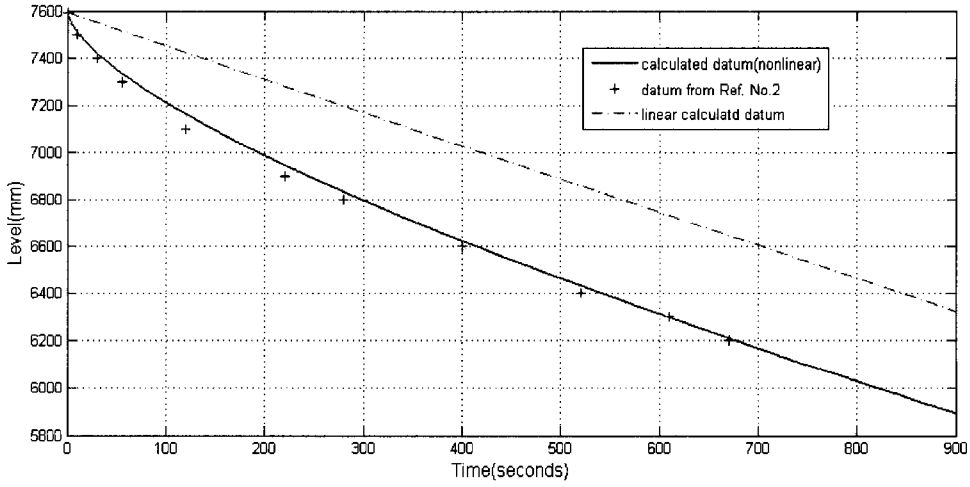


**Figure 2.7 Moderator levels compared at the leakage rate of 40 l/s**

## 2.3 The concepts of the fuel layers

Because most of the results in the following chapters will be shown as a function of moderator levels or of the leakage time, the following table, Table 2.6, will be convenient for engineering discussion and conclusions since it relates the moderator drop level to the reactor core layouts.

## 2.4 Moderator levels

In order to simulate the moderator level, the geometry will be changed with time by setting any materials above the moderator level to zero. These boundary changes will be detailed in the next chapter.

| Core | Moderator Level (top) | Moderator Level (bottom) |
|---|---|---|
| Top Reflector | 7594 | 7175 |
| Top Reflector | 7175 | 6940.25 |
| A | 6940.25 | 6654.5 |
| B | 6654.5 | 6368.75 |
| C | 6368.75 | 6083 |
| D | 6083 | 5797.25 |
| E | 5797.25 | 5511.5 |
| F | 5511.5 | 5225.75 |
| G | 5225.75 | 4940 |
| H | 4940 | 4654.25 |
| J | 4654.25 | 4368.5 |
| K | 4368.5 | 4082.75 |
| L | 4082.75 | 3797 |
| M | 3797 | 3511.25 |
| N | 3511.25 | 3225.5 |
| O | 3225.5 | 2939.75 |
| P | 2939.75 | 2654 |
| Q | 2654 | 2368.25 |
| R | 2368.25 | 2082.5 |
| S | 2082.5 | 1796.75 |
| T | 1796.75 | 1511 |
| U | 1511 | 1225.25 |
| V | 1225.25 | 939.5 |
| W | 939.5 | 653.75 |
| Reflector | 653.75 | 419 |
| Reflector | 419 | 0 |

**Table 2.6 Fuel layers (mm)**

# CHAPTER 3: SIMULATION ALGORITHM

## 3.1 Neutron calculation theory

### 3.1.1 Neutron diffusion equation

From the neutron balance, taking into account the reaction rates and independent neutron sources in a very small volume, the Boltzman neutron transport equations can be deduced. But, it is not possible to solve this equation for a real reactor core.

The diffusion equation for the whole reactor can be obtained from the P1 approximation to the transport equation. The main approximations are as follows [2]:

a) The angular flux has only one linear component of anisotropy;

$$\Phi\left(\vec{r},E,\vec{\Omega},t\right)=\frac{1}{4\pi}\left[\phi(\vec{r},E,t)+3\overrightarrow{\Omega}\cdot\vec{J}(\vec{r},E,t)\right] \qquad \text{EQ 3.1}$$

b) Neutron sources are isotropic.

With the above assumptions, we obtain the time and space dependent neutron flux equations which consist mainly of two related systems of partial differential equations: the first is the diffusion equation for the neutron flux, the second is the delayed neutron precursor equation. The complete matrix forms of system equations after energy condensation are as follows:

$$[v]^{-1}\frac{\partial}{\partial t}[\phi]=\nabla\cdot[D]\vec{\nabla}[\phi]-[\Sigma][\phi]+(1-\beta)[\chi^{P}]\frac{[\nu\Sigma_{f}]^{T}}{K_{eff}}[\phi]+\sum_{i=1}^{D}[\chi_{i}^{d}]\lambda_{i}C_{i} \qquad \text{EQ 3.2}$$

$$\frac{\partial}{\partial t}C_{i}=\beta_{i}[\nu\Sigma_{f}]^{T}[\phi]-\lambda_{i}C_{i} \qquad \text{EQ 3.3}$$

These parabolic equations with initial conditions and boundary conditions can only be solved analytically in two dimensions under very special assumptions. In three dimensions, these equations can only be solved with numerical methods. [12]

### 3.1.2 Static diffusion equation

From EQ 3.2 and 3.3, the following static diffusion equation is obtained:

$$-\nabla\cdot[D]\vec{\nabla}[\phi]+[\Sigma][\phi]=\frac{1}{Keff}[\chi^{P}][\nu\Sigma_{f}]^{T}[\phi] \qquad \text{EQ 3.4}$$

Using the spatial discretisation method, equation 3.4 can be set in a matrix form:

$$[A]\cdot[\Psi]=\frac{1}{Keff}[B]\cdot[\Psi] \qquad \text{EQ 3.5}$$

These equations are the key to static neutron calculations; the detailed forms of A and B are given in [12]. The usual solution technology is based on outer and inner iterations. The initial flux distribution and Keff will be solved by the outer loop; and then the new flux will be calculated by the inner loop. After the new flux is obtained, the new Keff will be calculated in the inner loop. The flux and Keff will be obtained when their relative error is small enough. The iteration for obtaining flux and Keff will stop once the

iteration error of the Keff and the flux is less than a specified value, set at 1E-6 in this work.

### 3.1.3 Kinetic equation

The mesh-centered, space-finite difference method is used on both static and kinetic neutron diffusion equation. The spatial mesh must be identical in both the static neutron calculations, which will serve as initial conditions for the kinetic neutron calculation, and the kinetic neutron calculations.

For mesh-centered finite differences, the required nuclear parameters (macroscopic cross sections and diffusion coefficients) will be constant in each mesh volume. In this method, only adjacent nodes are coupled by nodal leakages. These coupled equations lend themselves to the performance of numerical calculations; they have been proven to converge to the exact solution. The detail can be found in references [12] and [13].

A full implicit approximation for time derivative is used to solve the kinetic neutron equation. These detailed forms of the matrix [H] are in [12]. A matrix formulation of the equations is as follows:

$$\frac{\partial}{\partial t}[\Psi]=[H][\Psi] \qquad \text{EQ 3.6}$$

## 3.2 Neutron calculation practices

These simulations consist mainly of two parts: static neutron calculation and kinetic

neutron calculation. The static neutron calculation is used to calculate the initial static flux distribution and Keff. This distribution is then used to set up kinetic parameters at the beginning of the kinetic neutron calculation. The kinetic neutron calculation is performed through changing boundary conditions and the positions of reactivity control devices provided by the RRS modules.

### 3.2.1 Static part of neutron calculations

The flow chart of static neutron calculations is shown in Figure 3.1. Its functions can be described as follows:

a) The initialization of reactor geometry;
b) The set up of macro cross section of mixtures;
c) The calculation of neutron flux distribution, Keff and normalized total reactor power;
d) The set up of the reference readings of the reactor neutron power detection systems;
e) The initial set up of kinetic parameters for delayed neutron precursors;
f) The set up of the related RRS parameters.

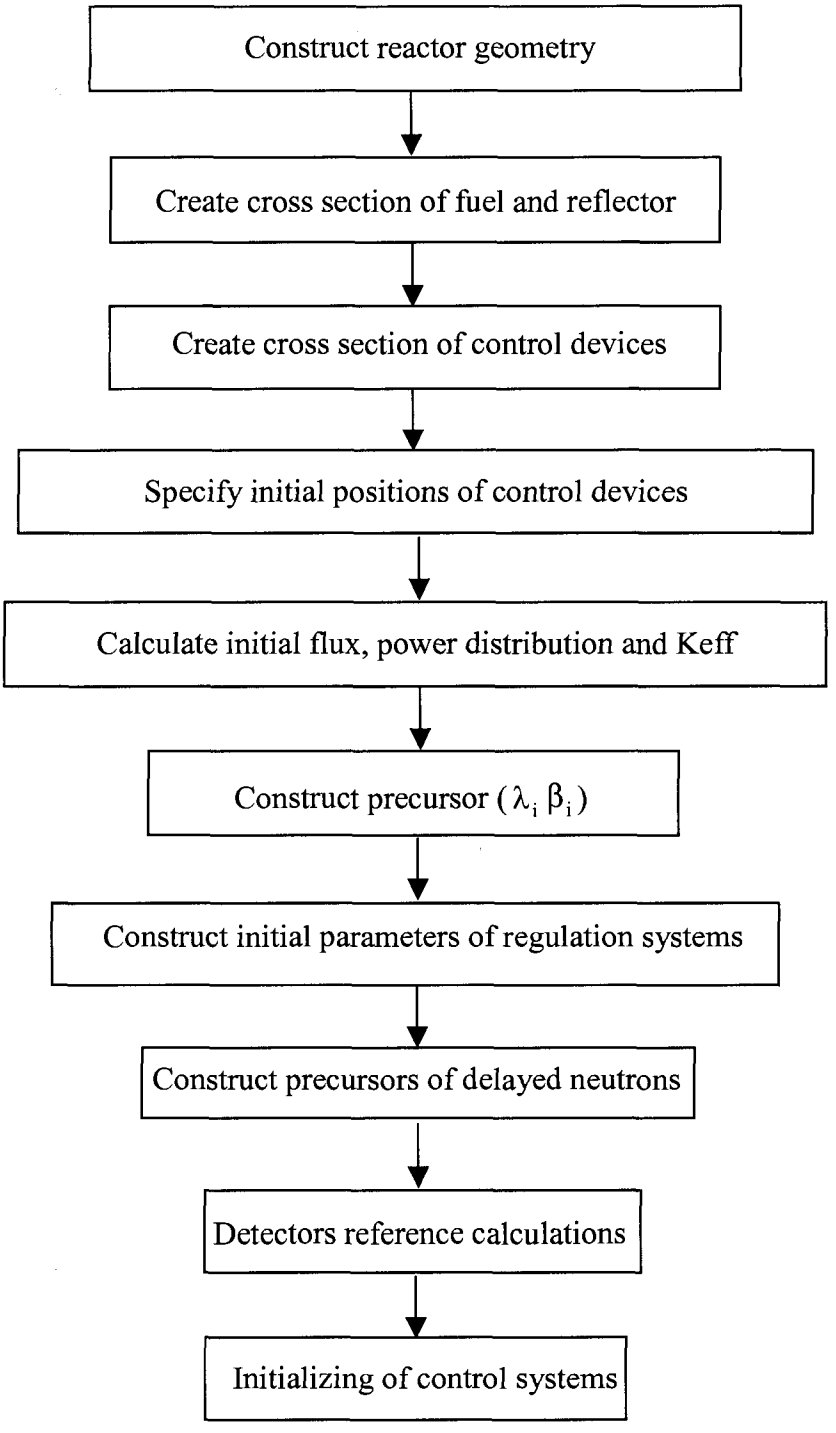


**Figure 3.1 Static part of neutron calculation**

### 3.2.1.1 Static parameters

The total power $P_{total}$ is used as the initial total reactor power in this simulation. It affects the initial flux amplitude along the whole reactor.

Six groups of delayed neutron precursors are used. The following equations are used in this calculation. Below is the initial concentration resulting from static calculation.

$$C_{i,n} = \frac{\beta_i}{\lambda_i} \left[\nu\Sigma_f\right]^T [\phi]_i \qquad \text{EQ3.7}$$

### 3.2.1.2 Geometry

Four sets of cross section in the reactor geometry have been obtained from the homogeneous burnup model. The fuel located in the central part is at a higher burnup than the fuel in the outer ring. The presence of the notch is properly accounted for. A typical plane for the geometry is shown in Figure 3.2.

Theoretically, mesh space can be restricted to a very small area, but our computer resources are limited. Also, more mesh split means a longer calculation time, sometimes requiring an unreasonably long computing time. A synthesis of accurancy and computing time has to be considered.

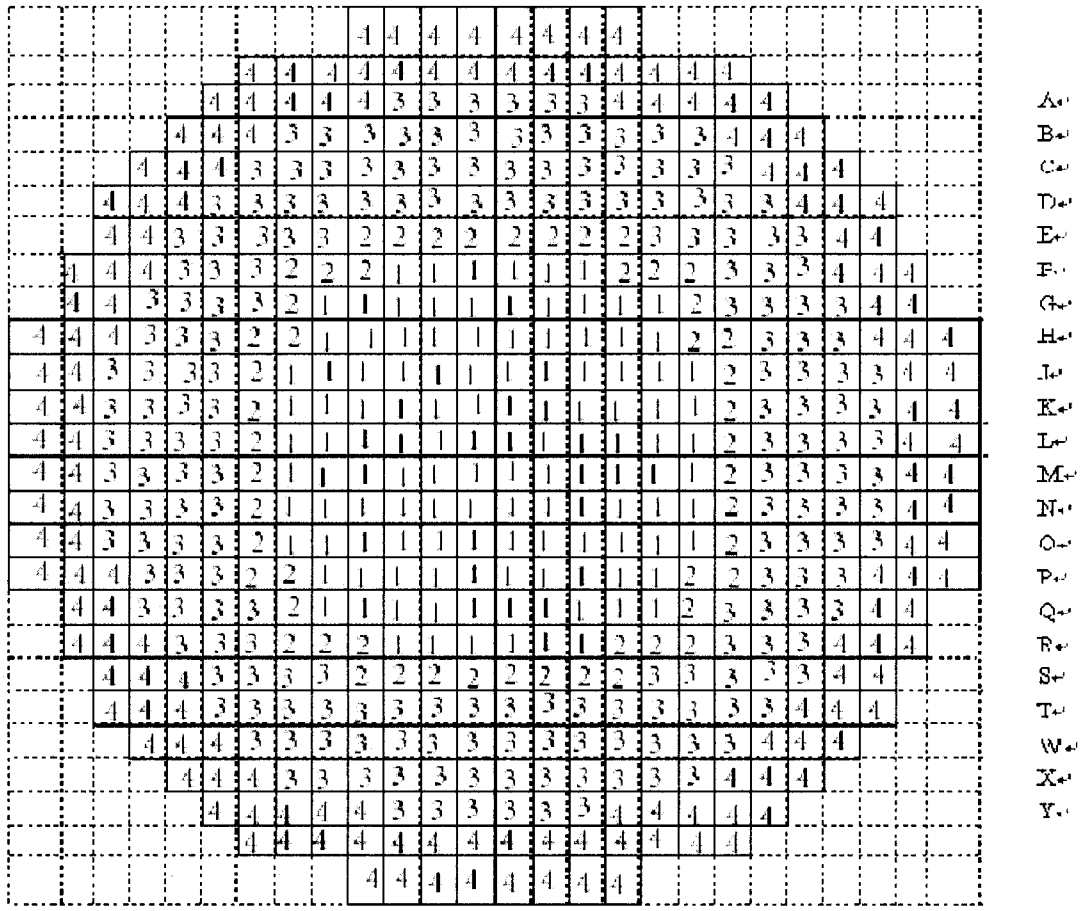

**Figure 3.2 Material indexes**

## 3.2.1.3 Set up of cross sections

DRAGON calculations provide macroscopic cross sections and diffusion coefficients along the fuel lattice and for the reflector, which will be used for the neutron diffusion equations in CANDU-6 reactor. [12]

We used the results from the DRAGON code as our properties of the fuels, reflector and different reactivity control devices.

#### 3.2.1.4 Set up of the reactivity control devices

Twenty-one adjusters were fully inserted in the reactor core, and fourteen liquid zone controllers were at initial levels (50% empty).

### 3.2.2 Kinetic part of neutron calculation

The space and time dependent diffusion equations were used in these simulations. A simple time average set of macroscopic cross sections, obtained from the DRAGON code [3], was used to represent the fuel conditions in the reactor core. The properties of the CANDU-6 reactivity control devices were also calculated with DRAGON [6]. The related kinetic part is shown in Figure 3.3.

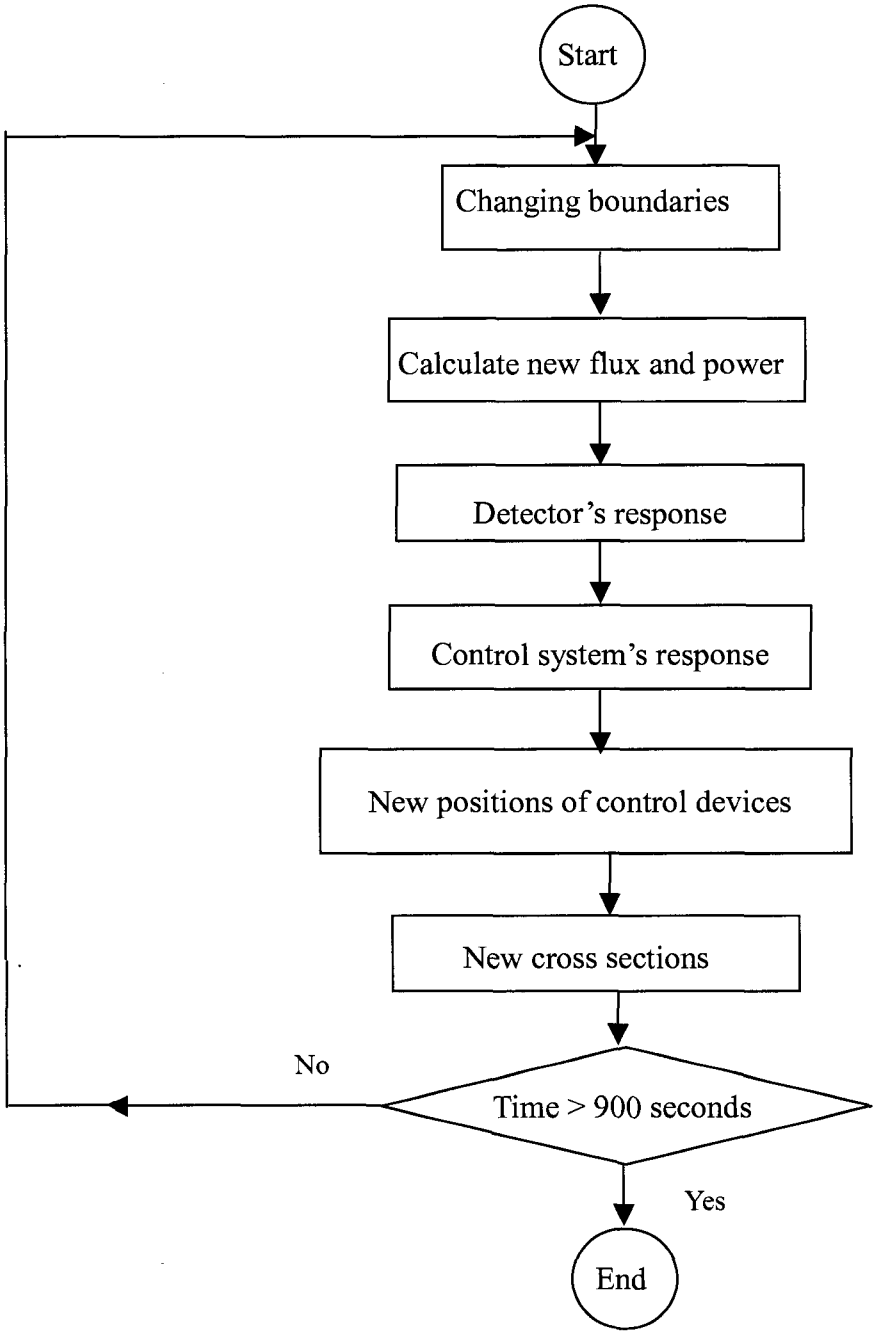


**Figure 3.3 Kinetic part of neutron calculations**

### 3.2.2.1 Kinetic parameters

MaxT will be used for determining a total leakage time in the kinetic calculation.

### 3.2.2.2 Detector reference readings calculation

Different neutron detectors have different responses to the input signals. The following three kinds of detectors were used in the CANDU-6 reactor simulation:

a) Three ion chambers were used for logarithmic power rates. Response time is fast.
b) Twenty-four Platinum detectors for zone power control. Response time is fast.
c) One hundred and two Vanadium detectors were used for flux mapping; the measured local powers are more accurate, but the response time is very slow.

For the Platinum detectors, the detector response codes have seven signal components. The prompt response of these detectors represents 84.5% of the signal. The remaining 15.5% are delayed, some of which are very long lived.

### 3.2.2.3 Control modules

Normally, the regulating systems have two important functions:

a) They will try to keep the reactor in a critical state and compensate for any power difference between the actual total reactor power and the requested total reactor power.

b) They will also maintain the fourteen zone control powers at their target values and avoid any serious power tilt.

### 3.2.3 Other considerations and assumptions

Because of the short simulation time (900 seconds) versus the very slow xenon response (8 hours), the xenon dynamic was not taken into account in our simulation.

Thermal feedback effects such as coolant density and temperature were not taken into account, nor were the effects of the fuel temperature and moderator temperature.

The moving boundary conditions were simulated by modifying the core geometry configuration at each time step (i.e. by changing material properties above the moving moderator level), taking into account the level reached by the moderator at different times due to the (constant) rates at which the moderator was being lost. The standard vacuum boundary conditions were applied to the moving moderator interface, which is a horizontal plane moving down. Accordingly, it was assumed that a vacuum exists above the moving moderator level and that neither fission reactions nor local power are generated above this moving moderator level. The moving boundary is shown in Figure 3.4.

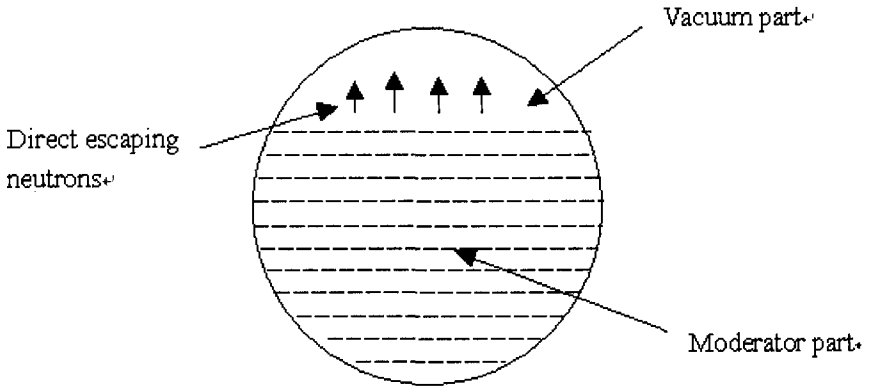


**Figure 3.4 Changing moderator level in a reactor core**

The boundary condition was implemented by setting to zero the material mixture above the moving moderator level. In a node, the vacuum space and the fuel space being 50% respectively, we could only bring to zero the whole node. This kind of approximation introduced some calculation errors.

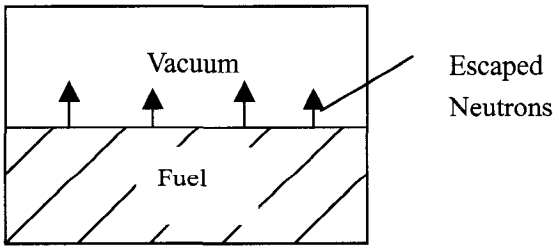


**Figure 3.5 Changing moderator level in a lattice**

As shown in the above figure, neutrons directly escape from the moderator level in this fuel lattice; this is understandable since very few neutrons reenter the fuel area from the vacuum area.

The current version of DRAGON used for the cross section generation in this work could not be used to calculate the macroscopic cross sections for the node above.

# CHAPTER 4: STATIC CALCULATIONS

## 4.1 Introduction to static calculations

Before a kinetic calculation problem is solved, a static calculation problem must be solved. This section will deal with a static neutron calculation in a CANDU-6 reactor. Even though a static neutron diffusion calculation is not one of the main objectives of this thesis, the related results will be helpful.

The basic three-dimensional model of a CANDU-6 reactor that we used is made up of a 26 x 26 x 12 mesh configuration along three axes y, x and z, which means that one cell corresponds to one mesh point. The four types of cells consist of three types of fuel and one reflector. It is a homogenous time average calculation with 2 types of fuel. One of higher burnup is in the center, and a lower burnup is located in outer core region. Two neutron energy groups and six delayed neutron precursor groups were used for the kinetic neutron calculations. A set of static calculations at a full power (2.18 E+09 Watts) level are shown in the following table.

| No. | Specification | Keff | Related Reactivity |
|---|---|---|---|
| 1 | No xenon/ adjusters fully inserted/zone level at 50% level | 1.024551 | 27 mk |
| 2 | With xenon/ adjusters fully inserted/zone level 50% level | 0.9970238 | 0 mk |
| 3 | No xenon/ adjusters fully inserted/zone level 0% level | 1.028255 | 30 mk |
| 4 | No xenon/ adjusters fully extracted/zone level 50% level | 1.03979957 | 41 mk |

**Table 4.1 Static Keff calculations**

Then, the reactivity of control devices or fission products is obtained from the above table as follows:

| Specification | Reactivity |
|---|---|
| Activity of xenon concentration | 27 |
| Activity of adjusters | 14 |
| Activity of zone controllers | 6 |

**Table 4.2 Reactivity of various control devices and xenon (mk)**

The calculated reactivity of xenon is very close to the results shown in [2]. The reactivity of the adjusters is also close to the results in [2]. The reactivity of the zone controllers lies between the value of [5] and [2]. For the control devices with smaller reactivity, the calculated error is a little higher.

## 4.2 Effective multiplication factor

Though the results obtained from the static neutron calculations are not suitable for kinetic neutron calculation, the results in Figure 4.1 do provide the guidelines for kinetic calculations.

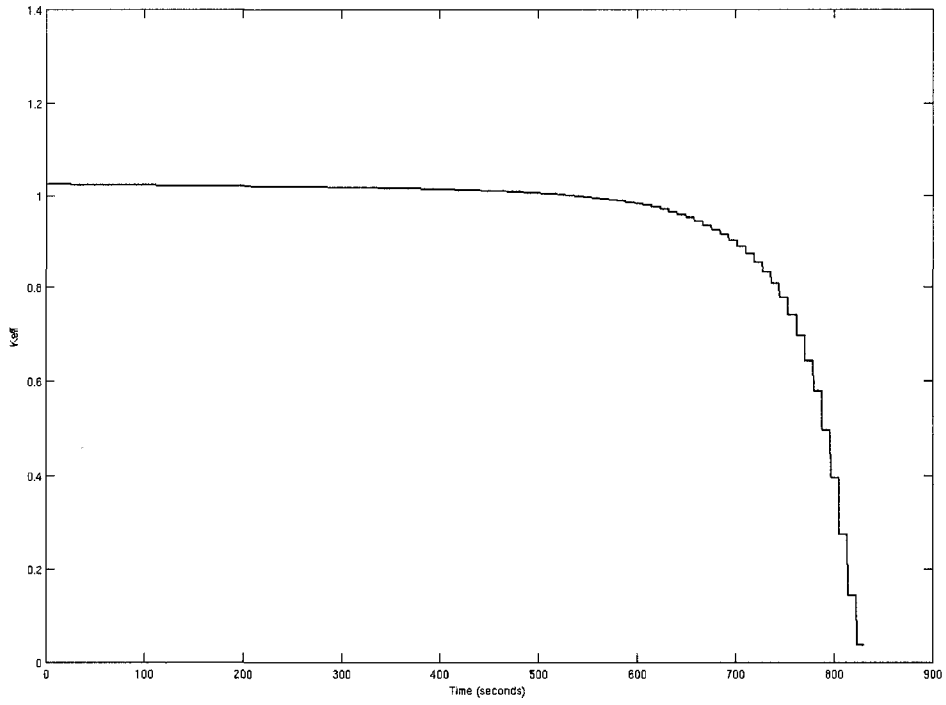


**Figure 4.1 Static Keff during a complete loss of moderator**

In obtaining the data of Figure 4.1, we assumed that the moderator in the entire reactor calandria would be lost completely during the 900 second transient. As expected, the Keff decreased with the moderator level. From this graph, we see that when the moderator level reached 3000 mm (from the top of calandria), the static Keff decreased quickly. The core became very sub-critical when fuel layer "M" reached zero and the moderator level dropped to a position below fifty percent of the calandria height. For the detail, see Figure 3.2.

All of our simulations lasted 900 seconds. Even for the fast moderator loss in a

CANDU-6 reactor, i.e. 122 l/s, the moderator level would only reach about fifty percent of the entire reactor calandria height during the 900 second transient.

In Figure 4.2 and 4.3, we suppose that the entire height of the reactor is normalized to 1. We can see the Keffs are always close to 1; also, Reactivity is close to 0.

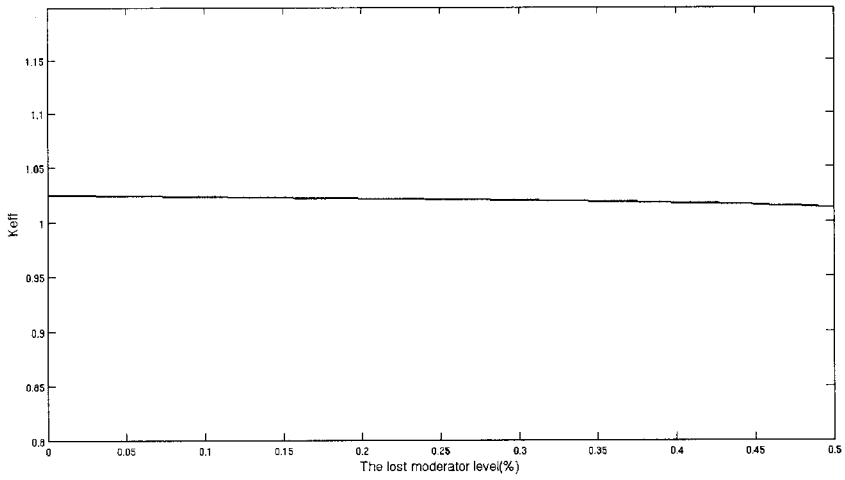


**Figure 4.2 Keff during 900 seconds with a loss of moderator**

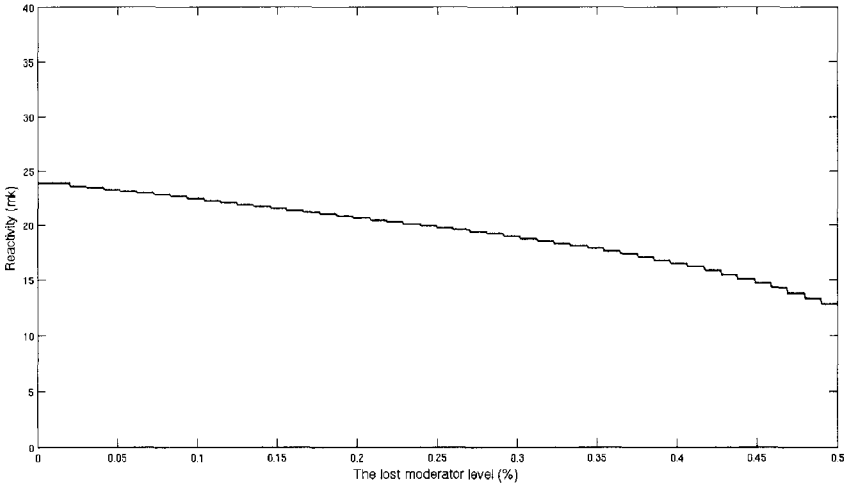


**Figure 4.3 Reactivity during 900 seconds with a loss of moderator**

# CHAPTER 5: KINETIC CALCULATIONS

## 5.1 Stability check

First, a series of space and time kinetic calculations were performed to check the stability of the system. The following configuration was used:

a) Xenon was set up at its equilibrium value;
b) Adjusters fully inserted;
c) Zone level at 50%.

Also, the influences of the following factors were examined:

a) Different splits;
b) Different time steps;
c) 900 second simulation;
d) No loss of moderator;

The results are shown in Figure 5.1. These results were obtained without the intervention of the reactor regulating system. A small error in the total reactor power gradually increased in time. This arose from rounding-off errors during the integration process; it may also have been related to internal data representation in the computer architecture.

The notation "split 16/2/2 0.25" means that every cell along the y axis is divided into sixteen smaller cells. Along the x and z axes, every cell is divided into two smaller cells. In total, there are four hundred and sixteen meshes along the y axis, fifty-two meshes

along the x axis and twenty-eight meshes along the z axis for the split "16/2/2". This indicates the size of our problem. A time step of 0.25 second was used for these simulations. From Figure 5.1, we see that more meshes in the reactor model led to a more stable calculated total reactor power during the 900 second transient.

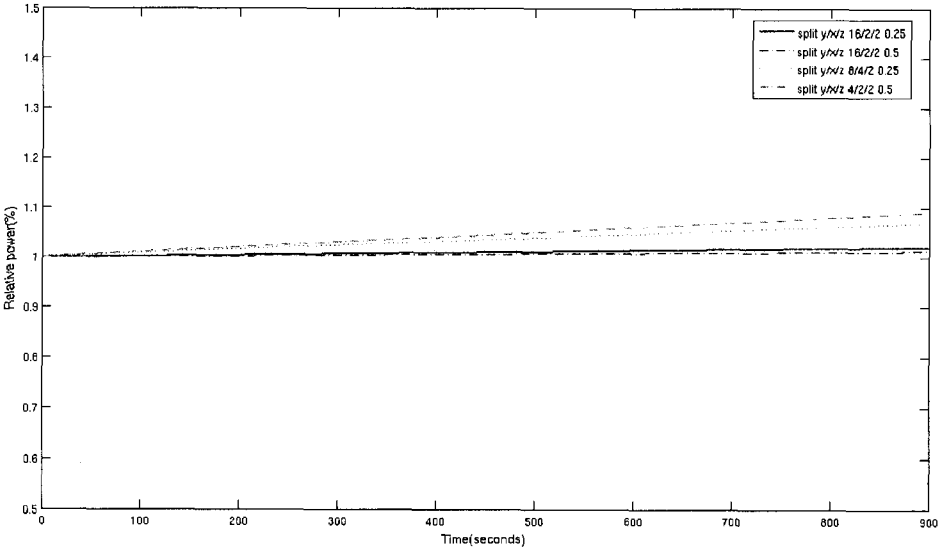


**Figure 5.1 Stability check without RRS**

Figure 5.2 shows that with the intervention of the reactor regulating system the calculated total reactor power was stable during this 900 second transient. This means that the reactor regulating system could compensate for the round off errors. Because the subsequent simulations needed to use the regulating function of zone liquid controllers, the results in Figure 5.2 are very important to this work. We can see that the calculated total reactor powers always had the same value, no matter which split and time steps were used. The liquid zone controllers moved somewhat to compensate for this total power

deviation.

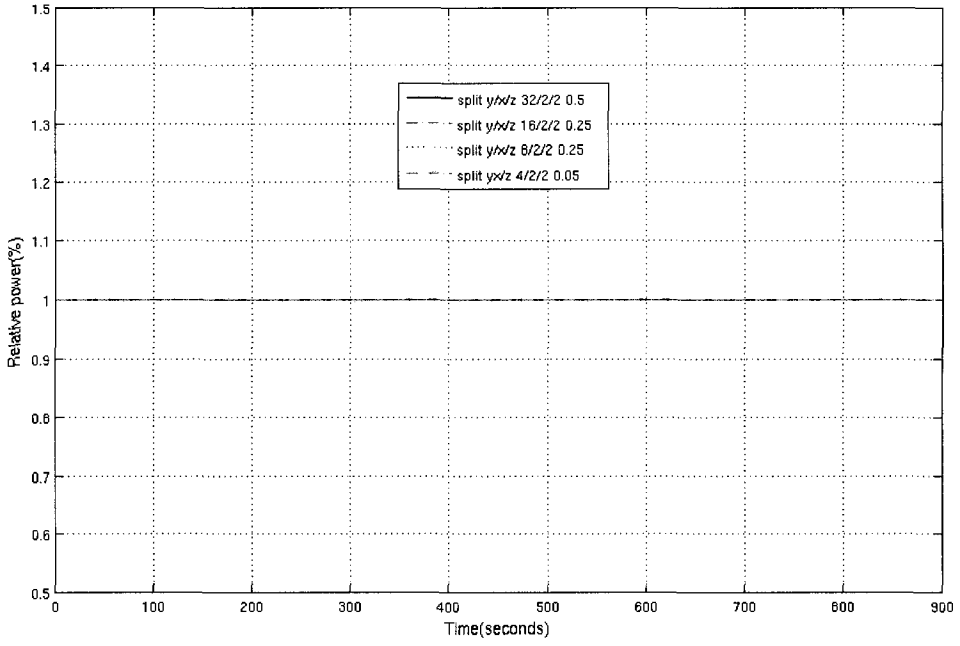


**Figure 5.2 Stability check with RRS**

## 5.2 Computing cost

The speed of calculation primarily depends on the performance of the computer hardware, system software and applications, and the number of concurrent users. Different computing times are required for different splits, as shown in Table 5.1. The computing time is basically proportional to the number of meshes.

| Split number | Number of meshes | Required time (Hours) |
|---|---|---|
| 13/2/2 | 421824 | 1.22 |
| 26/2/2 | 843648 | 2.14 |
| 52/2/2 | 1687296 | 3.55 |
| 104/2/2 | 3374592 | 6.14 |

**Table 5.1 Computing time**

## 5.3 Accuracy check

The accuracy of calculation depends on the number of mesh points in a calculation and the time steps. In Figure 5.3 and Figure 5.4, we notice some related calculation errors between different splits.

Theoretically, if a mesh space distance is less than $\frac{1}{\Sigma_t}$, it is a reasonable distance for the reactor neutron diffusion calculation. The detail refers to [14]. The infinitely small mesh space distance would be perfect; but taking into account this requirement and the limit of the computer's calculation capacity, the meshes 130x130x 120 (Split 5/5/5) were used as a reference and standard for calculations in the simulations.

In Figure 5.3, we can see that the results of different meshes are close to each other during this 900 second transient and that in the final moment of the transient, the results are closer than those at the middle moment.

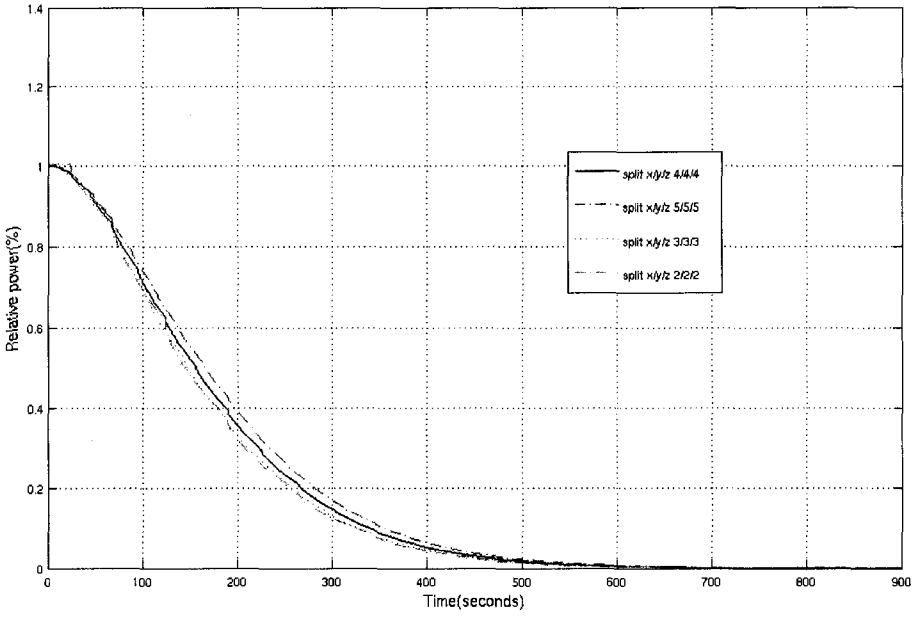


**Figure 5.3 Comparisons of calculation accuracy during 900 seconds**

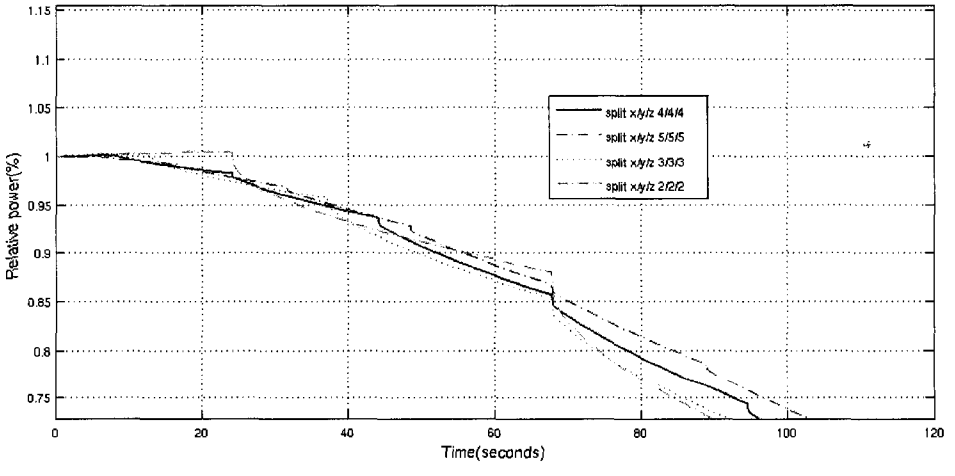


**Figure 5.4 Comparisons of calculation accuracy during 120 seconds**

From Figure 5.4, if we take the split 5/5/5 as our standard neutron calculation results, we find that the results from the split 4/4/4 are very close to those from the split 5/5/5. Therefore, the split 4/4/4 was used for the calculations in the rest of this work. In Table 5.2, the comparisons are given for different splits.

| Split number | $D_{avg}$ (%) | $D_{max}$ (%) | $P_{max\&cal}$ |
|---|---|---|---|
| 5/5/5 | 0 | 0 | 1.000774 |
| 4/4/4 | 1.12285 | 4.15733 | 1.002016 |
| 3/3/3 | 1.97056 | 7.09412 | 1.003332 |
| 2/2/2 | 2.06591 | 7.54317 | 1.005360 |

**Table 5.2 Comparisons of deviations**

$D_{avg}$ (%): Average deviation;

$D_{max}$ (%): Maximum deviation;

$P_{max\&cal}$: Ratio of maximum and calculated power;

We used the calculated results of the split 5/5/5 as our reference calculation; then we used:

$$\text{Deviation} = \frac{\text{Calculated value} - \text{Reference value}}{\text{Reference value}} \times 100\% \qquad \text{EQ5.1}$$

to get both average deviation and maximum deviation.

## 5.4 Selection of Operating Conditions

**Stepback:** the reactor stepback will drop MCA and adjusters down in reactor core once it is engaged. Finally the endpoint power will be 0% of full power.

**Setback:** the reactor setback will remain in force with the adjusters as long as the endpoint power has not been reached. Finally the endpoint power will be 60% of full power.

The STEPBACK function was not considered in order to avoid the resulting rapid decrease in total reactor power to zero. However, we did take the SETBACK function, adjusters and zone liquid controllers into account during our 900 second transient of the loss of moderator. In Table 5.3, four operating modes are detailed.

| Mode | Operating conditions |
|---|---|
| 1 | SETBACK inhibited, adjusters on manual |
| 2 | SETBACK inhibited, adjusters on auto |
| 3 | SETBACK operational, adjusters on manual |
| 4 | SETBACK operational, adjusters on auto |

**Table 5.3 Operating modes at 40 l/s**

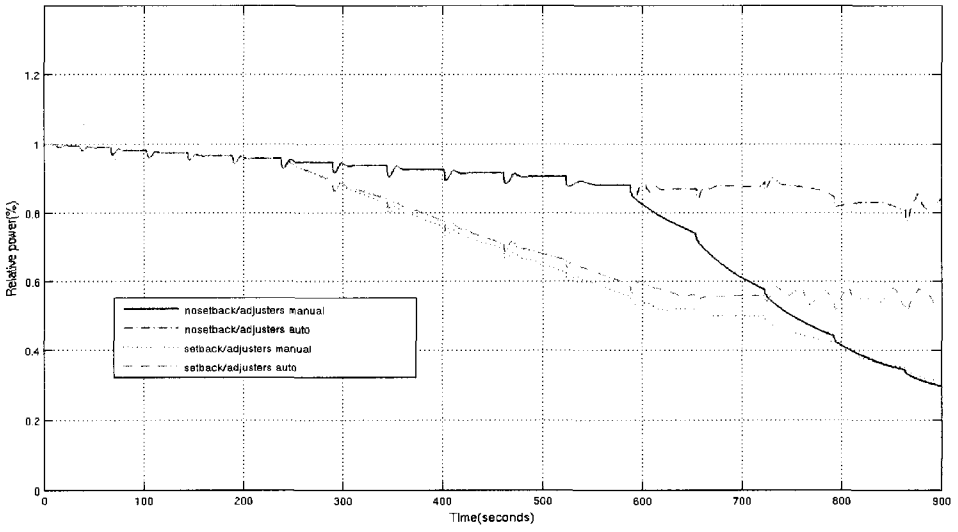


**Figure 5.5 Total reactor power variations at 40 l/s**

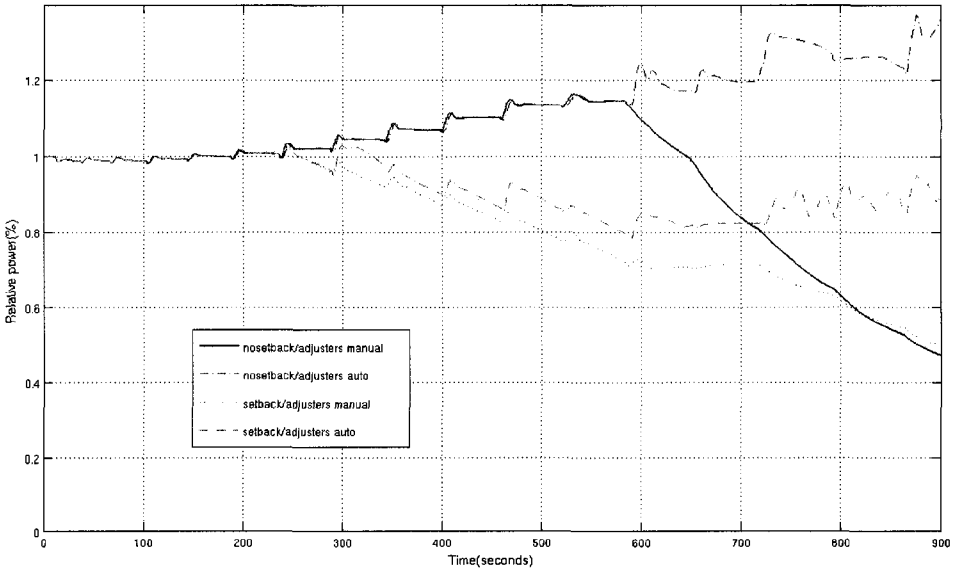


**Figure 5.6 Maximum bundle power variations at 40 l/s**

In Figure 5.5 and Figure 5.6, we find that the final total reactor power and maximum bundle power with adjusters on auto are double those with adjusters in manual mode. The compensations of adjusters play a very important role in the final moment of this 900 second transient.

Figure 5.5 shows that the total reactor power decreases during a loss of moderator.

We find that the maximum bundle power of the operating mode No. 2 will reach about 1.18 times the normal maximum bundle power, and the maximum bundle power of mode No. 4 will reach about 1.4 times the normal maximum bundle power. This means that the movement of the adjusters has an important impact on the local maximum bundle power during this transient. If the global control action is bigger than the partial local control action during the 900 seconds, a strong power distortion will occur at the bottom of the reactor. After the exhaustion of zone liquid controllers, the adjusters will affect the total reactor power significantly.

From the point of view of the maximum bundle power, operating mode No.1 and mode No.3 are safer for the normal operation of a CANDU-6 reactor.

Operating expenses in some CANDU-6 plants dictate that the adjusters are left in "manual" mode, the basic idea being that the adjusters are not expected to move when the reactor power is at a higher power. This avoids undesirable power peaks. For this reason, mode No.2 and No.4 were not considered.

In our simulations, the two shutdown systems and the automatic extraction of adjusters in a CANDU-6 reactor were restricted since once the two shutdown systems intervened, the

restart-up of CANDU-6 would be expensive. Mode 3 was, therefore, excluded. With the intervention of adjusters, the maximum bundle power during the transient exceeded 120% of its initial value. The detail is shown in Figure 5.6.

## 5.5 Different leakage rates

Various moderator leakage rates are possible: a loss of moderator lasts one hour to several hours inside a CANDU-6 reactor. In our study, five leakage rates were examined: 10 litres per second, 20 litres per second, 40 litres per second, 80 litres per second and 122 litres per second.

### 5.5.1 Comparison of total reactor powers

The variations of total reactor power during the 5 leakage rates are presented in Figure 5.7. The reactor power stayed above about 95% of normal total power during 900 seconds for the leakage rates of 10 l/s and 20 l/s. In these two cases, the level of moderator reached 6900 mm and 6600 mm respectively at 15 minutes. In Table 2.6, we find that a moderator level of 6900 mm corresponds to the top of the first fuel layer and that a level of 6600 mm is at the top of the second fuel layer. Therefore, we conclude that the total reactor power can be maintained near 100% of FPP after the moderator drops to the top part of the first and second fuel layers with the help of zone liquid controllers.

Figure 5.7 shows that, for the leakage rate of 122 l/s, the total reactor power is reduced significantly after 180 seconds; for the leakage rate of 80 l/s, the total reactor power will show an obvious decrease after 250 seconds; and for the leakage rate of 40 l/s, the total

reactor power decreases starting at the 580 second.

In Table 2.6, we find the following:

a) 122 l/s, 180 seconds, 6300 mm of moderator level, corresponds to the top of the third fuel layer,

b) 80 l/s, 250 seconds, 6350 mm of moderator level, corresponds to the top of the third fuel layer,

c) 40 l/s, 580 seconds, 6300 mm of moderator level, corresponds to the top of the third fuel layer.

In all cases, after the dropping moderator level reached the top of the third fuel layer, the total reactor power showed a power decrease. It can be concluded that the amount of fuel material plays an important part in the total reactor power. Obviously, after the first two fuel layers are reduced to zero, the total reactor power is decreased.

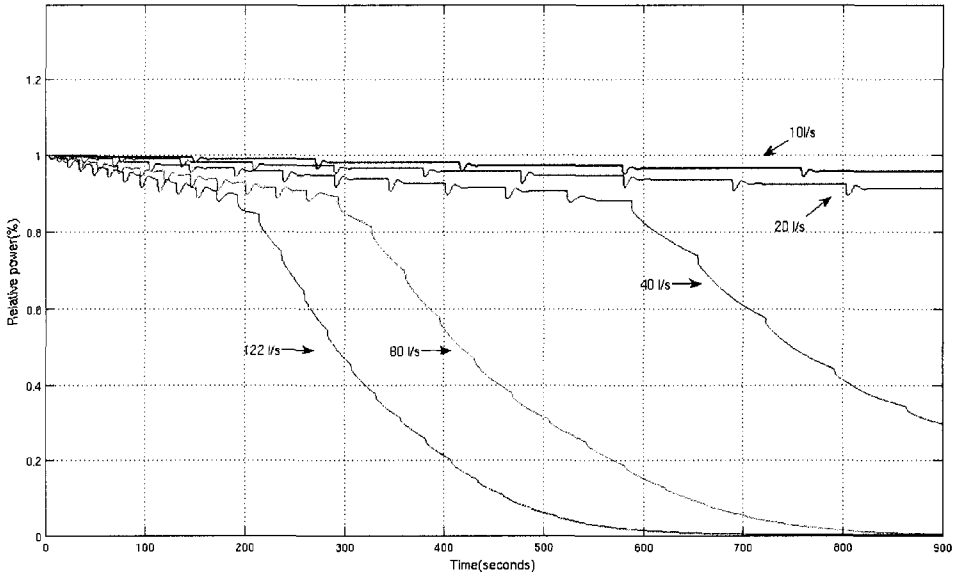


**Figure 5.7 Total reactor power as a function of time for different leakage rates**

Criticality can be maintained until the first two layers of fuel are lost, after which the total reactor can no longer be maintained at a critical state of FPP; therefore, total reactor power has a significant relationship to the quantity of moderator lost.

## 5.5.2 Comparison of maximum bundle powers

In a nuclear safety analysis, the maximum bundle power is an important parameter during the 900 second transient. The integral part of maximum bundle power curve above FPP line (i.e. the shaded area) is also important in reactor safety analysis as it is a measure of the severity of the bundle dry out risk during the transient.

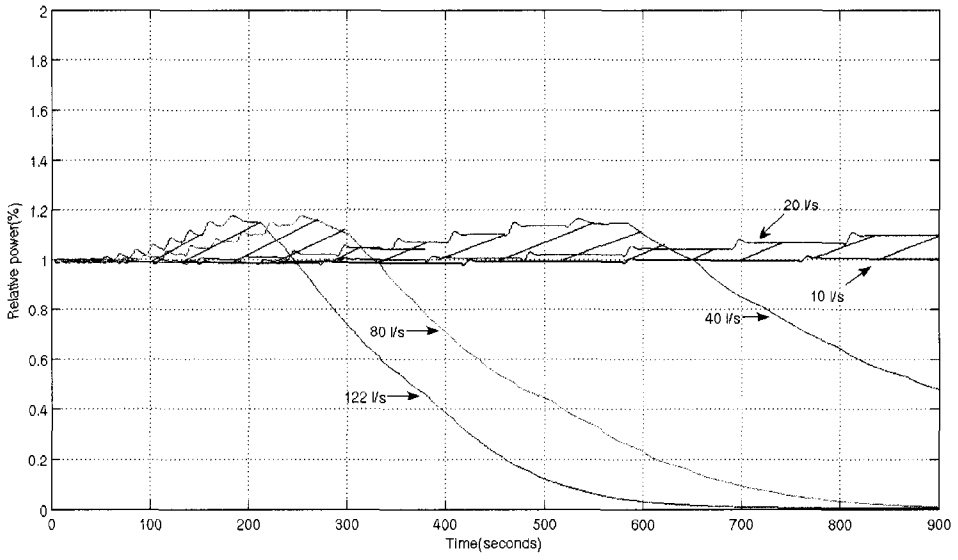


**Figure 5.8 Maximum bundle power variations of various leakage rates**

In Figure 5.8 it is also found that the maximum bundle power is reached at the moment the total reactor power starts decreasing at the top of the third fuel layer.

For the situations involving leakage rates at 10 l/s and 20 l/s, there is no significant increase of maximum bundle power.

## 5.6 Detailed RRS analysis

In this section, a set of results were analyzed for operating mode No.1 (split 4/4/4, no SETBACK function, no adjusters, only with liquid zone controllers). The leakage rate of 40 l/s, which is in middle of five rates, is typical of some plants. The detail refers to [1]

### 5.6.1 Power as a function of time

The total reactor power, maximum bundle power and maximum channel power for the leakage rate of 40 l/s are shown in Figure 5.9 and are representative of the behaviors observed in the other leakage rate situations.

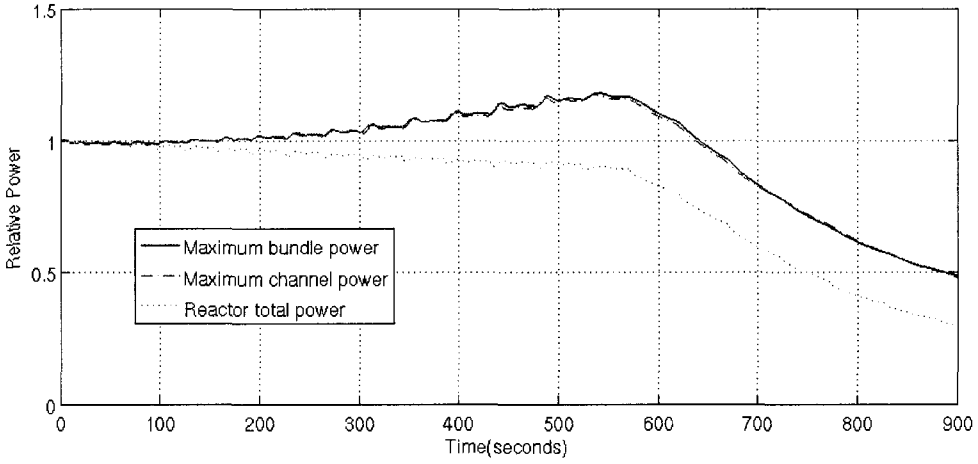


**Figure 5.9 Total reactor power, maximum bundle & channel powers (40 l/s)**

The total reactor power exhibits a tendency to decrease with time because of increased neutron losses through the enlarging surface created as the moderator is lost. The power rundown accelerates significantly at about 580s, when the first two layers of fuel have

been uncovered. At this moment, the positive reactivity of liquid zone controllers is exhausted. Also, the maximum bundle power and the maximum channel power decrease significantly at this time. Since the curve of the maximum bundle power exhibits the same behavior as that of the maximum channel power, we can use either of them to represent typical calculated results during the transients.

## 5.6.2 Zonal powers

The zonal power variation for zones 1 and 2 during the 900 seconds is illustrated in Figure 5.10. The regional power variation for zones 6 and 7 should be similar to this because of the symmetric layout of zones 6 and 7 with respect to zones 1 and 2. The details are shown in Figure1.4.

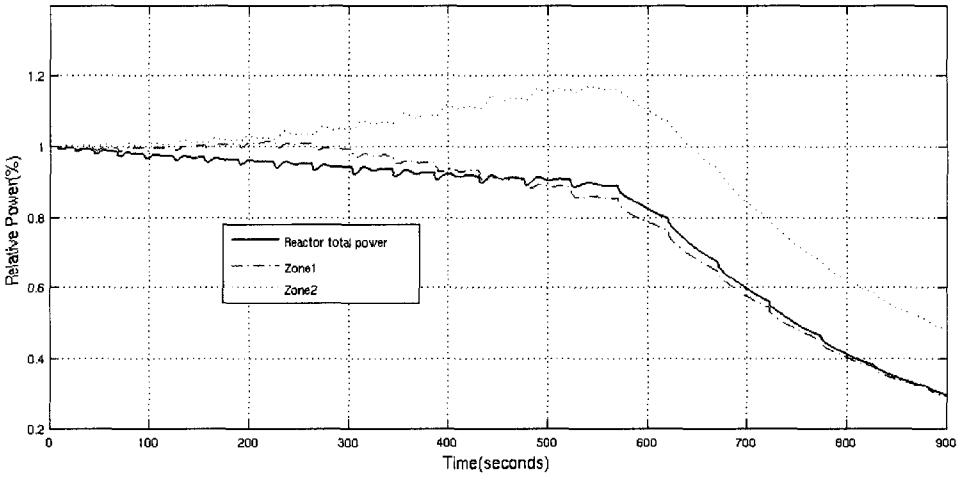

**Figure 5.10 Regional power variations of zone 1 and zone 2**

We observe that

a) The regional power decreases gradually during this transient;

b) A strong power increase occurs in zone 2, where the maximum zonal power reaches about 1.18 times its original value and exhibits behaviour similar to that of maximum bundle and channel powers during this transient.

c) The total reactor power decreases gradually to 30% of FPP.

Because of their symmetrical layouts, the power tendency of zone 10, 11, 12 is similar to that of zone 3, 4 and 5, which is shown in Figure 5.11.

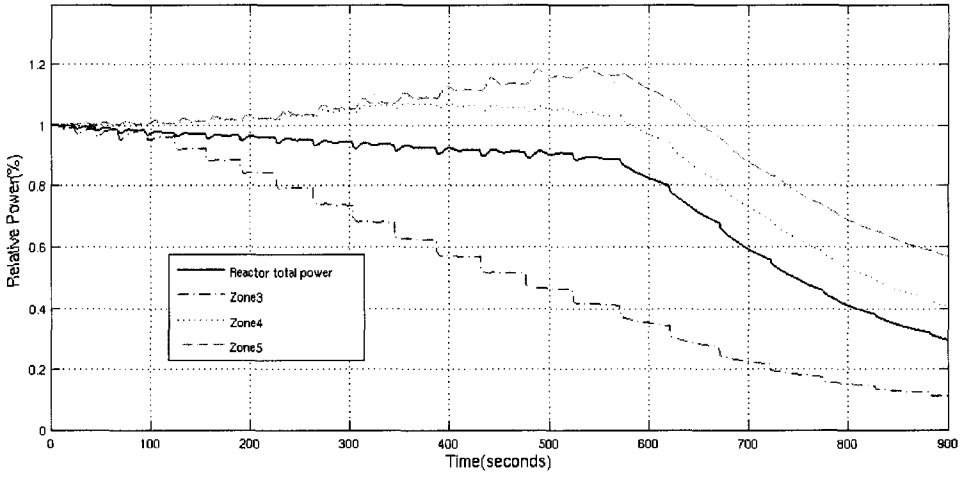


**Figure 5.11 Regional power as function of time of zone 3, 4 and 5 (40 l/s)**

Figure 5.11 shows that zone 5 has a stronger positive power increase than zone 4, whereas zone 3 shows a power decrease. This is because the actual loss of moderator occurs in the top of the core, thereby affecting zone 3, which will decrease in power despite the liquid zone controller in zone 3. The loss of power is compensated for by an increase in the power of the zones in the bottom of the core.

## 5.7 Flux distortion as a function of time

In our illustration of the flux distribution at different moments during the transient, the thermal flux in one plane only will be shown in order to emphasize the more important features of the transient. Plane 7 has been chosen because this is where some of the higher bundle powers occur during the fifteen minute transient.

The stable flux distribution of fast neutron and thermal neutrons are shown in Figure5.12 and Figure 5.13. These fluxes, presented at the beginning of the transient, are used as references for the transient calculations.

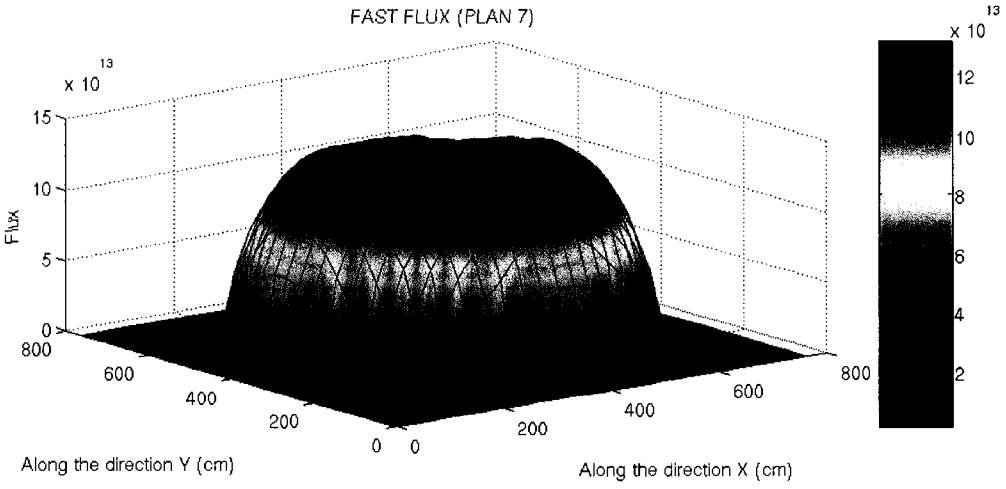


**Figure 5.12 Initial fast flux distribution of plane 7**

Both flux distributions show a good symmetrical layout which is lost during the transient.

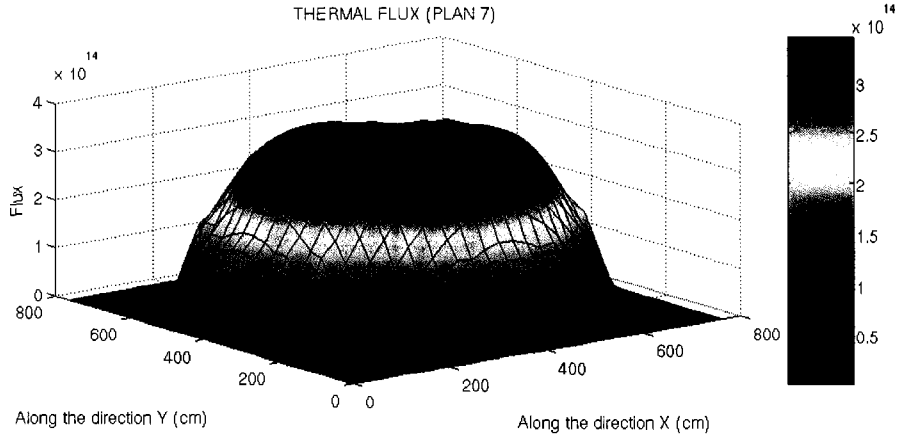


**Figure 5.13 Initial thermal flux distribution of plane 7**

A flux snapshot at 250 seconds into the transient is shown in Fig. 5.14. It is observed that the maximum thermal flux increased because of the drainage of zonal controllers.

The maximum thermal flux increased from $3.4\times10^{14}$ to $3.6\times10^{14}$. Compared to the initial flux shape, with the beginning of the loss of moderator and the interventions of liquid zone controllers, a slight flux distortion occurred.

Also, while the global control factor of RRS was still important in the process, the differential control factor was affecting the movement of the individual liquid zone controllers, as can be ascertained by examination of Fig 5.13 and Fig. 5.14.

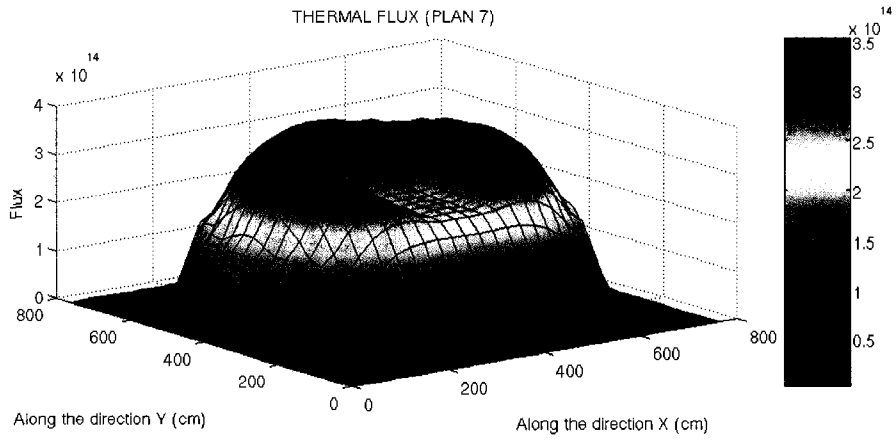


**Figure 5.14 Thermal flux distributions at 250.0 seconds**

Figures 5.15, 5.16 and 5.17 show the thermal flux distributions of plane 7 during a period of time when the maximum bundle power reached about 1.18 times its initial maximum bundle power.

We find that the maximum flux in plane 7 decreased between 488.0 seconds, illustrated in

Figure 5.15, and 500.0 seconds, shown in Figure 5.16. With the continuous decrease of liquid zones, the maximum flux of plane 7 at time t=535 increased again, as shown in Figure 5.17, due to the competition between the loss of moderator and the falling zone levels.

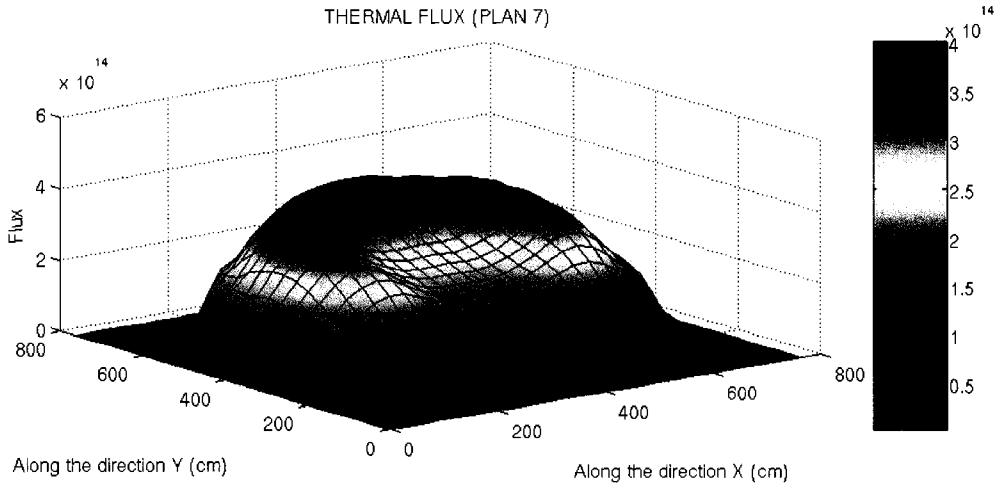


**Figure 5.15 Thermal flux distributions at 488.0 seconds**

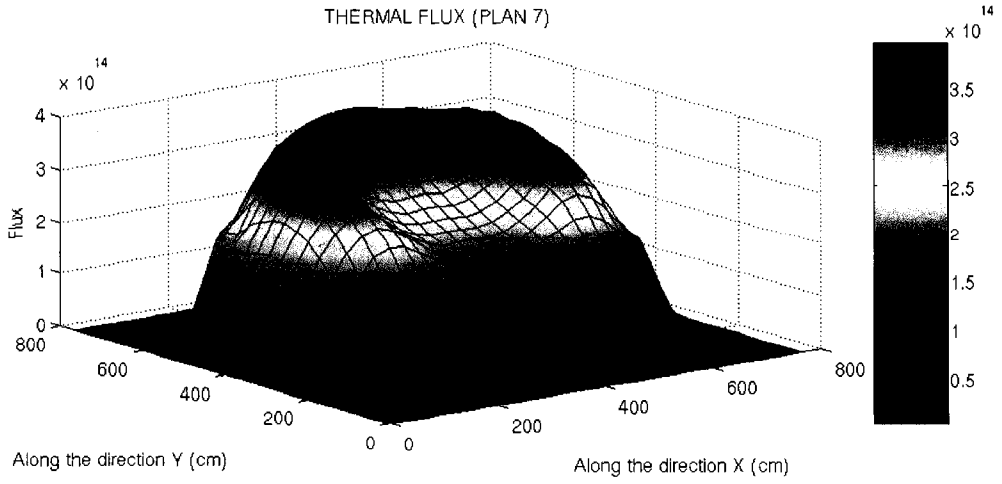

**Figure 5.16 Thermal flux distributions at 500.0 seconds**

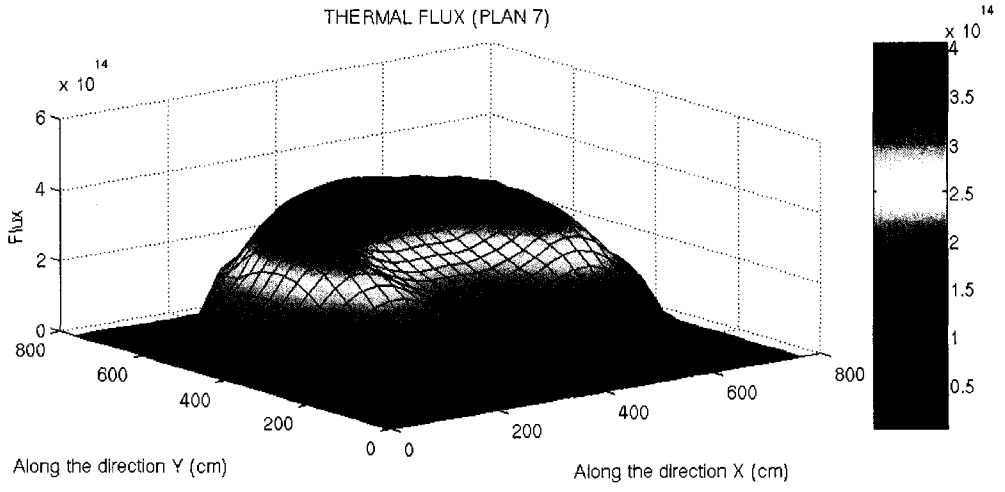


**Figure 5.17 Thermal flux distributions at 535.0 seconds**

After about 550 seconds, the maximum flux of plane 7 started to decrease significantly. In Figures 5.18 and 5.19, it is observed that a strong flux distortion occurred, although we must take into account that the actual flux values were much lower than at previous times because the effect of the liquid zone controllers was essentially negligible: they had reached such low values that no further significant flux increase could be achieved by them.

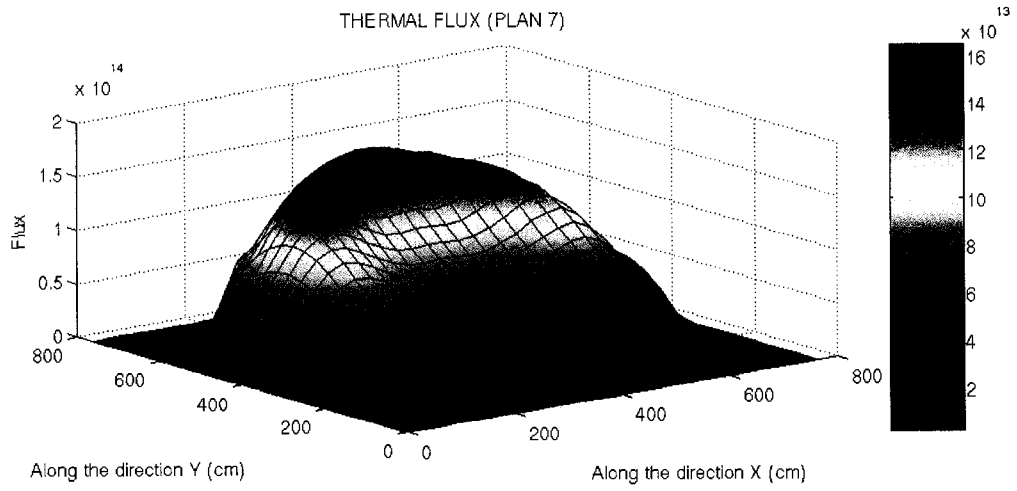


**Figure 5.18 Flux distributions at 750.0 seconds**

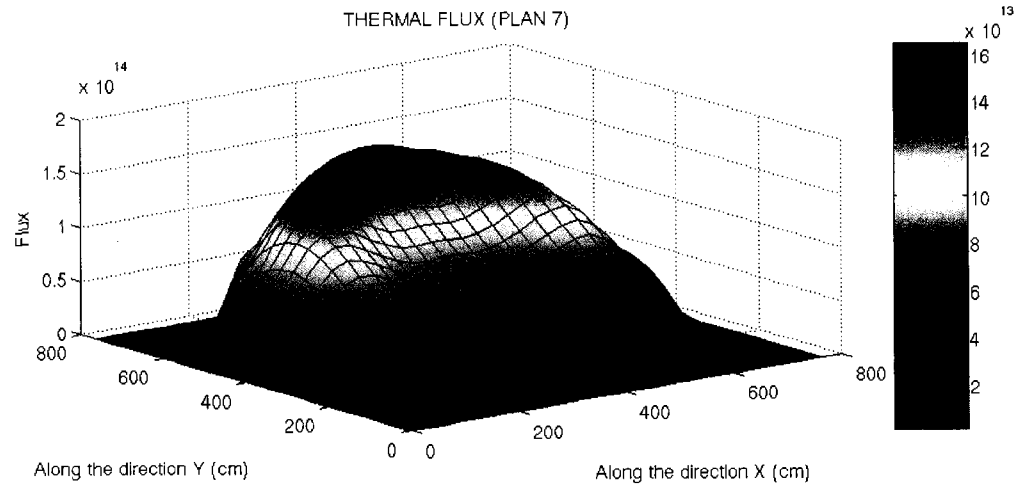


**Figure 5.19 Flux distributions at 900.0 seconds**

## 5.8 Zone level

Figures 5.20 and 5.21 show that all the zone controllers were at minimal levels at the end of this transient. This means that almost all of the liquid zone controllers were emptied during this transient.

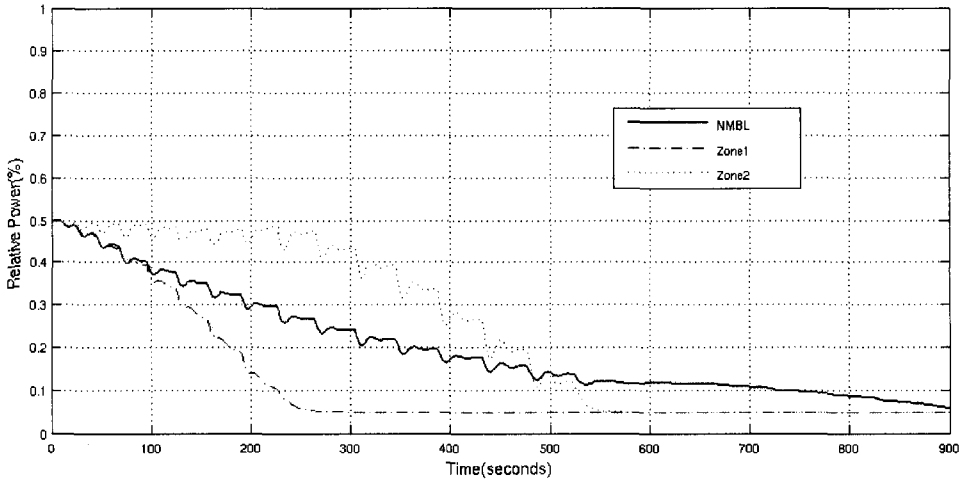


**Figure 5.20 Zone level as function of time in zones 1 and 2**

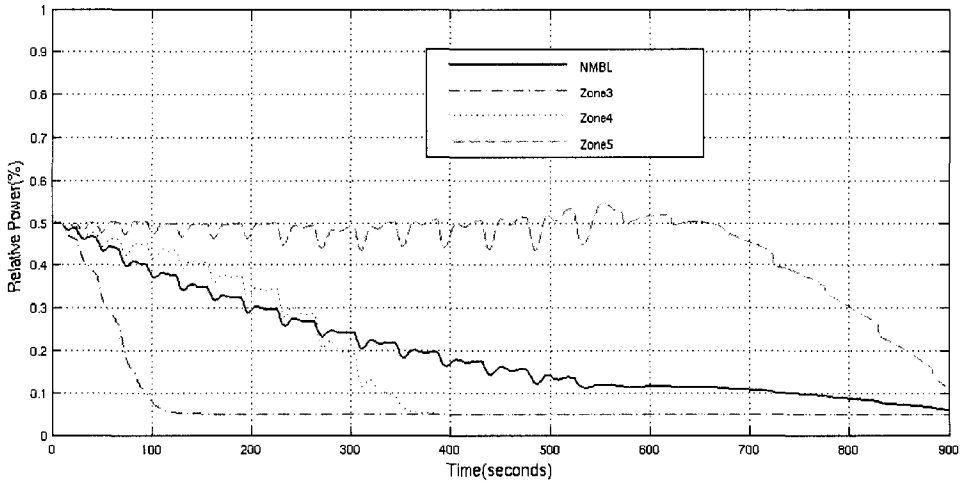


**Figure 5.21 Zone level as function of time in zones 3, 4 and 5**

In Figure 5.21 we can see that the zone level decreased more slowly in the lower part of the reactor core because the power in these zones were not affected by the loss of moderator affecting the top of the core and, therefore, the reactor's top zones. At the end of the transient, the liquid zone controllers were almost exhausted. This means that the reactivity of the moderator loss was greater than the reactivity of the zone level change.

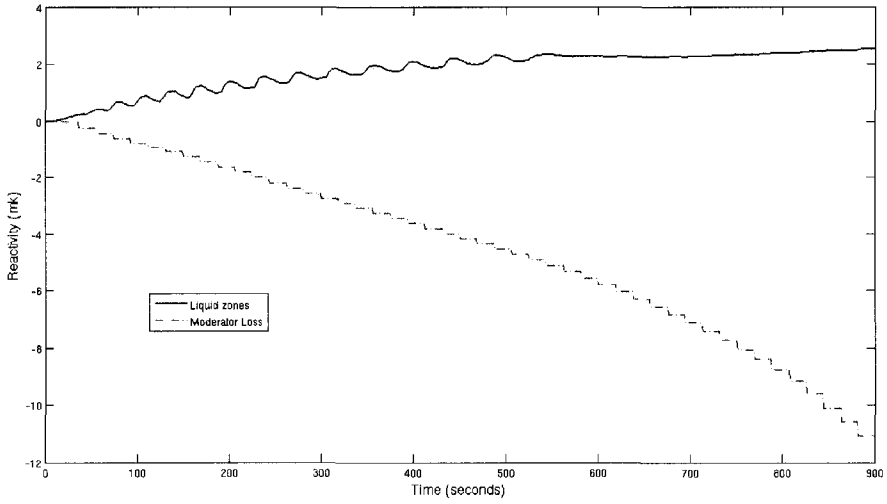


**Figure 5.22 Reactivity change of zone controllers and moderator loss**

# CHAPTER 6: CONCLUSIONS AND RECOMMENDATIONS

## 6.1 Conclusions

For a typical moderator leakage rate, without the STEPBACK and SETBACK functions, and adjusters on manual mode, we can conclude that

a) The total reactor power decreases rapidly when the moderator level descends below the first two fuel layers;
b) The maximum bundle and maximum channel values do not exceed 1.18 times their initial value. This means that the risk of dryout is very small;
c) The moment at which the maximum bundle power and maximum channel power are reached is similar to the moment at which a total power decrease starts. At that moment, the reactivity from the liquid zone controllers has been exhausted.

For smaller moderator leakage rates, the dryout risk is much less than for a large moderator leakage rate.

For large moderator leakages rates, the maximum bundle and channel power during this transient will be the same, i.e. 1.18 times their initial value. This means that only the peak value of bundle and channel power will be sensitive to the reactivity compensation.

## 6.2 Recommendations

a) An error arising between the continuous moderator level and the discrete model level used here will affect the intervention moment of the regulating system. The splits will also introduce error into this simulation. We have used a split of 5/5/5. A study of even finer mesh would be of interest;

b) A power variation calculation of moderator loss under realistic conditions should be performed.

# REFERENCES


1. Jean Koclas, « Jean Koclas Private communication », August 1993, Quebec, Canada.
2. Rozen Daniel, « Introduction to Nuclear Reactor Kinetics », Institut de génie nucléaire, École polytechnique de Montréal, Montréal, Polytechnique International Press, Canada, April 1998.
3. G. Marleau, A. Hébert and R. Roy, « A User's Guide for DRAGON », Technical Report IGE- 174 Rev. 3, École Polytechnique de Montréal, December (1997).
4. « ENDF-B VI », Evaluated Nuclear Data Library, Nuclear Energy Agency (1990)
5. Koclas, J., « Reactor Control and Simulation », Simulation Lectures Note, École polytechnique de Montréal, Montréal, Canada, 1996.
6. R. Roy, G. Marleau, J. Tajmouati and D. Rozon, « Modeling of CANDU Reactivity Control Devices with the Lattice Code DRAGON », *Annals of Nuclear Energy*, **21**, pp. 115-132 (1994).
7. E. Varin, A. Hébert, R. Roy and J. Koclas, « A User Guide For Donjon Version 2.01 », IGE-208, Institut de génie nucléaire, École polytechnique de Montréal, Montréal, Canada, May 2000.
8. S. Kaveh, J. Koclas, R. Roy, « Space-Time Kinetics Calculations Using a Multigrid Acceleration Technique », *Proceedings of the PHYSOR 2000*, Pittsburgh, PA, May 2000.
9. J. Koclas, B. Forget, « CANDU Reactor Simulations with a Full P1 Method », *Proceedings of the PHYSOR 2004*, Chicago, April 25-29, IL USA.
10. S. Kaveh, Jean Koclas, Robert Roy, « Nuclear Reactor Kinetics Using Hierarchical Super Nodal Analysis », *Proceedings International Conference on Mathematics*

*and Computation, Reactor Physics and Environmental Analysis in Nuclear Applications*, Madrid, Spain, September 1999.

11. Henry, Alan, F., « Nuclear Reactor Analysis », MIT Press, Cambridge, Mass, USA, 1975
12. Koclas, J., « Reactor Neutron Analysis », Lectures Note, École polytechnique de Montréal, Montréal, Canada, 1996.
13. KAVEH-KHORIE Siamak, « Nuclear Reactor Kinetics Based on Hierarchical Nodal Analysis », Ph.D. Thesis, École polytechnique de Montréal, Montréal, Canada, 2000.
14. Samuel Glasstone and Alexander Sesonske, « Nuclear Reactor Engineering », U.S. Department of Energy, Malabar, Florida, USA, 1991.